

Precision SUSY Measurements at LHC*

I. Hinchliffe^a, F.E. Paige^b, M.D. Shapiro^a, J. Söderqvist^c, and W. Yao^a

^a*Lawrence Berkeley National Laboratory, Berkeley, CA*

^b*Brookhaven National Laboratory, Upton, NY*

^c*Royal Institute of Technology (KTH), Stockholm, Sweden*

Abstract

If supersymmetry exists at the electroweak scale, then it should be discovered at the LHC. Determining masses, of supersymmetric particles however, is more difficult. In this paper, methods are discussed to determine combinations of masses and of branching ratios precisely from experimentally observable distributions. In many cases such measurements alone can greatly constrain the particular supersymmetric model and determine its parameters with an accuracy of a few percent. Most of the results shown correspond to one year of running at LHC at “low luminosity”, $10^{33} \text{ cm}^{-2} \text{ s}^{-1}$.

arXiv:hep-ph/9610544v1 30 Oct 1996

*This work was supported in part by the Director, Office of Energy Research, Office of High Energy and Nuclear Physics, Division of High Energy Physics of the U.S. Department of Energy under Contracts DE-AC03-76SF0009 and DE-AC02-76CH00016 and by the Swedish National Research Council.

Contents

1	Introduction	2
2	Effective Mass Analysis	5
3	LHC Point 3: $m_0 = 200$ GeV, $m_{1/2} = 100$ GeV, $\tan \beta = 2$	11
3.1	Measurement of $M_{\tilde{\chi}_2} - M_{\tilde{\chi}_1}$	11
3.2	Gluino and Sbottom Reconstruction	11
3.3	Light Squark Reconstruction	12
3.4	Branching ratio of $\tilde{\chi}_2 \rightarrow \tilde{\chi}_1^0 \ell^+ \ell^-$	13
3.5	Electroweak Production of Superpartners	13
4	LHC Point 4: $m_0 = 800$ GeV, $m_{1/2} = 200$ GeV, $\tan \beta = 10$	20
4.1	Selection of gaugino decays $\tilde{\chi}_i \rightarrow \tilde{\chi}_j \ell^+ \ell^-$	20
4.2	Selection of $\tilde{\chi}_4^0 \rightarrow \tilde{\chi}_1^\pm W^\mp \rightarrow e^\pm \mu^\mp X$	21
5	LHC Point 5: $m_0 = 100$ GeV, $m_{1/2} = 300$ GeV, $\tan \beta = 2.1$	27
5.1	Selection of $h \rightarrow b\bar{b}$ and Measurement of $M(\tilde{u}_L) - M(\tilde{\chi}_1^0)$	27
5.2	Selection of $W \rightarrow q\bar{q}$ and Measurement of $M(\tilde{u}_L) - M(\tilde{\chi}_1^0)$	28
5.3	Selection of $\tilde{\chi}_2^0 \rightarrow \tilde{\ell} \ell \rightarrow \tilde{\chi}_1^0 \ell \ell$	29
5.4	Top Production in SUSY Events	30
6	LHC Points 1, 2: $m_0 = m_{1/2} = 400$ GeV, $\tan \beta = 2, 10$	38
6.1	Selection of $h \rightarrow b\bar{b}$ and Measurement of $M(\tilde{u}_L) - M(\tilde{\chi}_1^0)$	38
6.2	Selection of $\tilde{\chi}_i \rightarrow \tilde{\chi}_j \ell^+ \ell^-$	38
7	Determining SUSY parameters	43
7.1	LHC Point 3	43
7.2	LHC Point 5	44
7.3	LHC Point 4	46
7.4	LHC Points 1 and 2	47
8	Conclusions	51

1 Introduction

If supersymmetry (SUSY) exists at the electroweak scale, then gluinos and squarks will be copiously produced in pairs at the LHC and will decay via cascades involving other SUSY particles to the lightest SUSY particle (LSP), the $\tilde{\chi}_1^0$. In most models the $\tilde{\chi}_1^0$ is stable, must be neutral and therefore escapes the detector. It should then be easy to observe deviations from the Standard Model such as an excess of events with multiple jets plus missing energy \cancel{E}_T or with like-sign dileptons $\ell^\pm\ell^\pm$ plus \cancel{E}_T [1, 2, 3]. Determining SUSY masses is more difficult because each SUSY event contains two LSP's, and there are not enough kinematic constraints to determine the momenta of these.

The strategy developed in Ref. [4] and in this paper involves three steps. First, we use a simple inclusive analysis to establish a deviation from the Standard Model. We select events with at least four jets and large missing energy and plot the distribution of

$$M_{\text{eff}} = p_{T,1} + p_{T,2} + p_{T,3} + p_{T,4} + \cancel{E}_T.$$

Typically, this is dominated by Standard Model processes at low M_{eff} but is a factor of 5–10 larger than the Standard Model prediction for large M_{eff} . The value of M_{eff} at which the signal exceeds that standard model backgrounds provides a first estimate of the SUSY masses.

The second step in the strategy is to identify characteristic signatures of particles occurring near the end of the SUSY decay cascades and to use these as the starting point for further analysis. This is best explained by an example. Suppose that gluinos are slightly heavier than squarks and that $\tilde{\chi}_2^0 \rightarrow \tilde{\chi}_1^0 h$ is kinematically allowed. Then one can have the following decay chain:

$$\begin{array}{cc}
 \tilde{g} & + \tilde{g} \\
 \downarrow & \downarrow \\
 \tilde{q}_L + \bar{q} & \tilde{q}_R + \bar{q} \\
 \downarrow & \downarrow \\
 \tilde{\chi}_2^0 + q & \tilde{\chi}_1^0 + q \\
 \downarrow & \\
 \tilde{\chi}_1^0 + h & \\
 \downarrow & \\
 b + \bar{b} &
 \end{array}$$

Such an event typically contains two hard jets from the $\tilde{q}_{L,R}$ decays, two b jets from the h decay, large \cancel{E}_T , and soft jets from the gluino decays and from gluon radiation. In this case, one can reconstruct $h \rightarrow b\bar{b}$ as a peak in the $b\bar{b}$ mass distribution and measure its mass [5]. Then the h can be combined with either of the two hard jets. The smaller of these two masses must be less than the squark mass and so has a sharp edge that measures a known function of the \tilde{q}_L , $\tilde{\chi}_2^0$, and $\tilde{\chi}_1^0$ masses. In many cases several such measurements can be made to determine several combinations of masses more or less precisely.

Given actual data, the third step would be to make a global fit of a SUSY model to all available measurements, including both the precision measurements just described and more inclusive ones such as the jet, lepton, and b -jet multiplicities and p_T distributions. Such an analysis involves simulating large numbers of signal samples and is beyond the scope

Table 1: SUGRA parameters for the five LHC points.

Point	m_0 (GeV)	$m_{1/2}$ (GeV)	A_0 (GeV)	$\tan \beta$	$\text{sgn } \mu$
1	400	400	0	2.0	+
2	400	400	0	10.0	+
3	200	100	0	2.0	-
4	800	200	0	10.0	+
5	100	300	300	2.1	+

of this study. Instead, we try to determine the SUSY parameters using just the precision measurements of combinations of masses. In some cases this almost completely determines the SUSY model, while in others it significantly constrains it.

What precision measurements can be made is very dependent on the SUSY model and so must be studied for specific SUSY parameters. The ATLAS and CMS Collaborations at the LHC have been considering five points in the minimal supergravity (SUGRA) model listed in Table 1 [4]. The SUGRA model [6] has the minimal SUSY particle content; universal scalar masses m_0 , gaugino masses $m_{1/2}$, and trilinear breaking terms A_0 at the grand unification scale; and radiative electroweak symmetry breaking driven by the large top quark mass. After electroweak breaking, the remaining parameters are a ratio of vacuum expectation values $\tan \beta$ at the weak scale and a sign, $\text{sgn } \mu = \pm 1$. We assume a default value for the top quark mass of 175 GeV and comment on the sensitivity to it below. While this model may not be the one that nature has chosen, we would like to emphasize that simulations can only be performed in the context of a consistent model. This is because many promising signals that might be clearly distinguished from Standard Model backgrounds in one channel, can be obscured by production and decays of other supersymmetric particles. We may not believe in this model, but the model that nature has chosen will be self-consistent.

In the SUGRA model, if $\tilde{\chi}_2^0 \rightarrow \tilde{\chi}_1^0 h$ is kinematically allowed, it has a substantial branching ratio and provides one starting point. This is the case for LHC Points 1, 2, and 5. If this decay is kinematically forbidden, then in many cases $\tilde{\chi}_2^0 \rightarrow \tilde{\chi}_1^0 \ell^+ \ell^-$ can be observed. This is the case for LHC Points 3 and 4. The endpoint of the $\ell^+ \ell^-$ mass distribution provides a direct measure of $M(\tilde{\chi}_2^0) - M(\tilde{\chi}_1^0)$, and opposite-sign, same-flavor dileptons can be used to identify events containing $M(\tilde{\chi}_2^0)$. Other modes exploited in this paper include $\tilde{\chi}_2^0 \rightarrow \tilde{\ell}_R^\pm \ell^\mp \rightarrow \tilde{\chi}_1^0 \ell^\pm \ell^\mp$ and $\tilde{\chi}_4^0 \rightarrow \tilde{\chi}_1^\pm W^\mp \rightarrow \tilde{\chi}_1^0 e^\pm \mu^\mp \nu \bar{\nu}$.

All the analyses presented here are based on isajet 7.22 [7] and a toy detector simulation. At least 50k events were generated for each signal point. The standard model background samples contained 250k events for each of $t\bar{t}$, WZ with $W \rightarrow e\nu, \mu\nu, \tau\nu$, and Zj with $Z \rightarrow \nu\bar{\nu}, \tau\tau$, and 5000K QCD jets (including g, u, d, s, c , and b) divided among five bins covering $50 < p_T < 2400$ GeV. The calorimeter energy resolutions are taken to be

$$\begin{aligned}
 \text{EMCAL} & 10\%/\sqrt{E} + 1\% \\
 \text{HCAL} & 50\%/\sqrt{E} + 3\% \\
 \text{FCAL} & 100\%/\sqrt{E} + 7\%, \quad |\eta| > 3.
 \end{aligned}$$

A uniform segmentation $\Delta\eta = \Delta\phi = 0.1$ is used with no transverse shower spreading. This is particularly unrealistic for the forward calorimeter. Jets are found using GETJET [7] with a fixed cone size $R = 0.4$ or 0.7 . Missing transverse energy is calculated by taking the magnitude of the vector sum of the transverse energy deposited in the calorimeter cells. The jet multiplicity in SUSY events is rather large, so we will use a cone size of 0.4 unless otherwise stated. A lepton efficiency of 90% and a b -tagging efficiency of 60% is assumed. Isolated leptons are required to satisfy an isolation requirement that no more than 10 GeV of additional E_T be present in a cone of radius $R = 0.2$ around the lepton. Results are presented for an integrated luminosity of 10 fb^{-1} , corresponding to one year of running at $10^{33} \text{ cm}^{-2}\text{s}^{-1}$ so pileup has not been included. We will occasionally comment on the cases where the full luminosity of the LHC, *i.e.* $10^{34} \text{ cm}^{-2}\text{s}^{-1}$, will be needed to complete the studies. For many of the histograms shown, a single event can give rise to more than one entry due to different possible combinations. When this occurs, all combinations are included.

In Section 2 of this paper, we discuss using M_{eff} to get a rough estimate of SUSY masses. We then turn to more detailed analyses. In these, we shall usually make cuts so that the Standard Model backgrounds are very small. These cuts are not optimal, particularly in the case of the higher mass points where event rates are lower. It may be desirable to have more signal events at the cost of more background. In Sections 3 and 4 we discuss LHC Points 3 and 4 respectively. These points have rather light gauginos, so $\tilde{\chi}_2^0 \rightarrow \tilde{\chi}_1^0 \ell^+ \ell^-$ can be used to measure $M(\tilde{\chi}_2^0) - M(\tilde{\chi}_1^0)$. In Section 5 we discuss LHC Point 5, which has both $\tilde{\chi}_2^0 \rightarrow \tilde{\chi}_1^0 h \rightarrow \tilde{\chi}_1^0 b \bar{b}$ and $\tilde{\chi}_2^0 \rightarrow \tilde{\ell}^\pm \ell^\mp \rightarrow \tilde{\chi}_1^0 \ell^\pm \ell^\mp$. In Section 6 we briefly discuss LHC Points 1 and 2. These have gluino and squark masses of about 1 TeV, so they really need more than 10 fb^{-1} for detailed study. In Section 7 we investigate how well the precision measurements discussed determine the parameters of SUSY model. Finally, we draw some conclusions.

2 Effective Mass Analysis

The first step in the search for new physics is to discover a deviation from the Standard Model and to estimate the mass scale associated with it. SUSY production at the LHC is dominated by gluinos and squarks, which decay into multiple jets plus missing energy. A variable which is sensitive to inclusive gluino and squark decays is the effective mass M_{eff} , defined as the scalar sum of the p_T 's of the four hardest jets and the missing transverse energy \cancel{E}_T ,

$$M_{\text{eff}} = p_{T,1} + p_{T,2} + p_{T,3} + p_{T,4} + \cancel{E}_T.$$

Here the jet p_T 's have been ordered such that $p_{T,1}$ is the transverse momentum of the leading jet. The Standard Model backgrounds tend to have smaller \cancel{E}_T , fewer jets and a lower jet multiplicity. In addition, since a major source of \cancel{E}_T is weak decays, large \cancel{E}_T events in the Standard Model tend to have the missing energy balanced by leptons. To suppress these backgrounds, the following cuts were made:

- $\cancel{E}_T > 100 \text{ GeV}$;
- ≥ 4 jets with $p_T > 50 \text{ GeV}$ and $p_{T,1} > 100 \text{ GeV}$;
- Transverse sphericity $S_T > 0.2$;
- No μ or isolated e with $p_T > 20 \text{ GeV}$ and $\eta < 2.5$;
- $\cancel{E}_T > 0.2M_{\text{eff}}$.

With these cuts and the idealized detector assumed here, the signal for all five LHC points is much larger than the Standard Model backgrounds for large M_{eff} , as is illustrated in Figures. 1–5.

The peak of the M_{eff} mass distribution, or alternatively the point at which the signal (S) begins to exceed the standard model background (B), provides a good first estimate of the SUSY mass scale, which is defined to be

$$M_{\text{SUSY}} = \min(M_{\tilde{g}}, M_{\tilde{u}_R})$$

While M_{SUSY} obviously should be set by the gluino and squark masses, the choice of $M_{\tilde{u}_R}$ as the typical squark mass is somewhat arbitrary. The ratio of the value M_{eff} for which

Table 2: The value of M_{eff} for which $S = B$ compared to M_{SUSY} , the lighter of the gluino and squark masses. Note that Point 3 is strongly influenced by the \cancel{E}_T and jet p_T cuts.

LHC Point	M_{eff} (GeV)	M_{SUSY} (GeV)	Ratio
1	1360	926	1.47
2	1420	928	1.53
3	470	300	1.58
4	980	586	1.67
5	980	663	1.48

$S = B$ to M_{SUSY} was calculated by fitting smooth curves to the signal and background and is given in Table 2. It must be noted, however, that for LHC Point 3 the cuts produce a minimum value of M_{eff} near the crossover. A more realistic treatment of the \cancel{E}_T resolution could be important for this point. At this point event rates are so large that this step in our procedure is not needed; we will not use \cancel{E}_T in the analyses shown below.

To see whether the approximate constancy of this ratio might be an accident, 100 SUGRA models were chosen at random with $100 < m_0 < 500$ GeV, $100 < m_{1/2} < 500$ GeV, $-500 < A_0 < 500$ GeV, $1.8 < \tan\beta < 12$, and $\text{sgn}\mu = \pm 1$. These models were compared to the assumed signal, LHC Point 5. The light Higgs was assumed to be known, and all the comparison models were required to have M_h within ± 3 GeV of its nominal value; the 3 GeV error is determined not by the experimental measurements but by an estimate of the theoretical uncertainties on the prediction of M_h from the parameters of the SUGRA model. A sample of 1K events was generated for each point, and the peak of the M_{eff} distribution was found by fitting a Gaussian near the peak. Figure 6 shows the resulting scatterplot of M_{SUSY} vs. M_{eff} . The ratio is constant within about $\pm 10\%$, as can be seen from Figure 7. The mean value of the ratio is higher here than in Table 2 because this analysis uses the peak of the distribution rather than the point at which it is equal to the background. The error on the ratio is conservative, since there is considerable contribution to the scatter from the limited statistics and the rather crude manner in which the peak was found. While M_{eff} does not provide a precise measurement, it has the advantage of being generally applicable to a broad range of SUSY models.

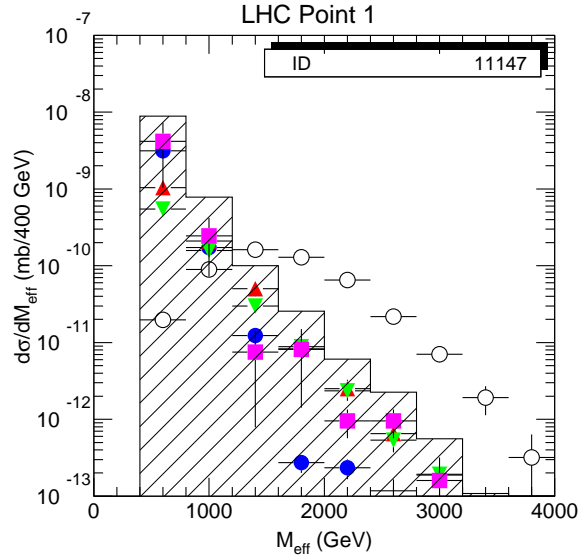


Figure 1: LHC Point 1 signal and Standard Model backgrounds. Open circles: SUSY signal. Solid circles: $t\bar{t}$. Triangles: $W \rightarrow \ell\nu, \tau\nu$. Downward triangles: $Z \rightarrow \nu\bar{\nu}, \tau\tau$. Squares: QCD jets. Histogram: sum of all backgrounds.

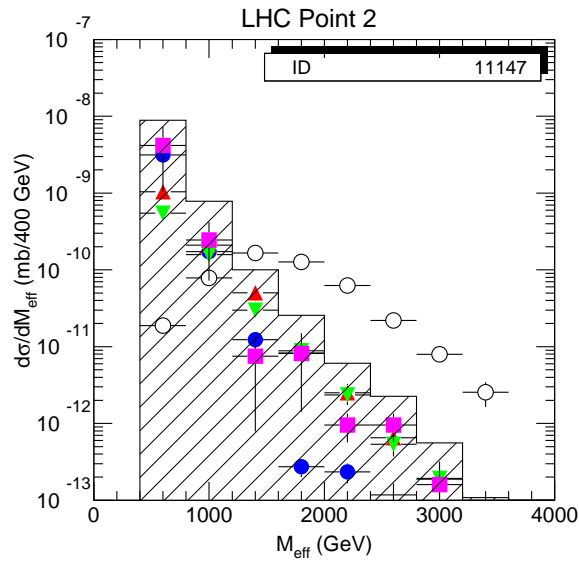


Figure 2: SUSY signal and Standard Model backgrounds for LHC Point 2. See Figure 1 for symbols.

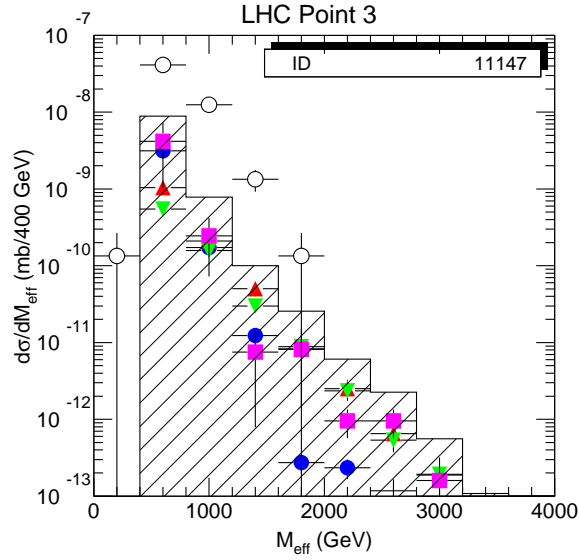


Figure 3: SUSY signal and Standard Model backgrounds for LHC Point 3. See Figure 1 for symbols.

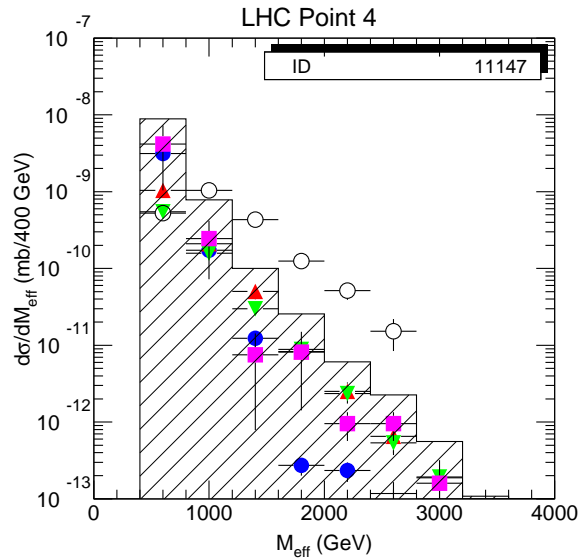


Figure 4: SUSY signal and Standard Model backgrounds for LHC Point 4. See Figure 1 for symbols.

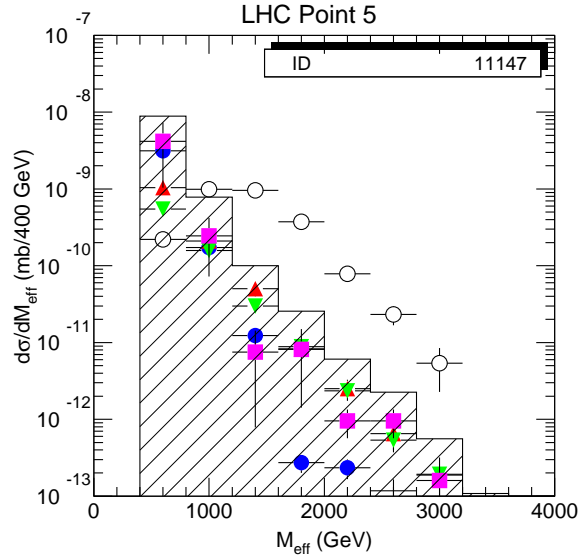


Figure 5: SUSY signal and Standard Model backgrounds for LHC Point 5. See Figure 1 for symbols.

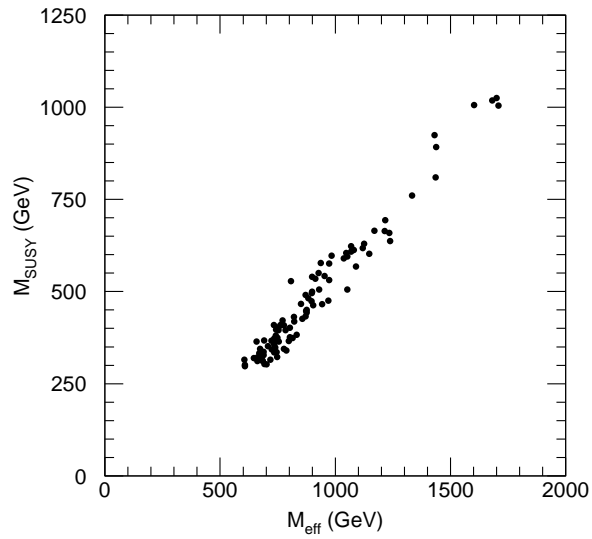


Figure 6: Scatterplot of $M_{\text{SUSY}} = \min(M_{\tilde{g}}, M_{\tilde{u}})$ vs. M_{eff} for randomly chosen SUGRA models having the same light Higgs mass within ± 3 GeV as LHC Point 5.

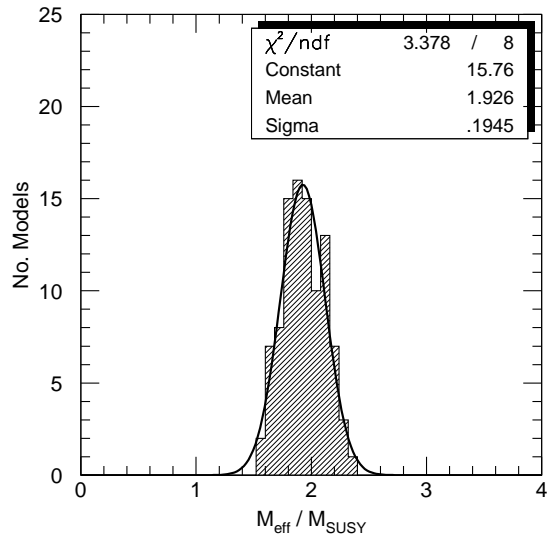


Figure 7: Ratio $M_{\text{eff}}/M_{\text{SUSY}}$ from Figure 6. The distribution of this ratio is approximately Gaussian with a width about 10% of its mean.

3 LHC Point 3: $m_0 = 200 \text{ GeV}$, $m_{1/2} = 100 \text{ GeV}$, $\tan \beta = 2$

LHC Point 3 has relatively light superpartners and hence a very large production rate. At this point 200,000 events were generated, corresponding to about 1 week of LHC running at low luminosity; the statistical fluctuations on the plots are due to this small Monte Carlo sample. All of the squarks of the first two generations are heavier than the gluino, but one of the stop and sbottom mass eigenstates is lighter than the gluino while the other is heavier. The dominant SUSY production process is $\tilde{g}\tilde{g}$, and the dominant gluino decay mode is $\tilde{g} \rightarrow \tilde{b}\bar{b}$. The lightest \tilde{b} is mainly \tilde{b}_L and so decays principally into $b\tilde{\chi}_2^0$ since $\tilde{\chi}_2^0$ ($\tilde{\chi}_1^0$) is mainly \tilde{W}_3 (\tilde{B}). Then $\tilde{\chi}_2^0$ decays via virtual sleptons to $\tilde{\chi}_1^0 e^+ e^-$ with a 16% branching ratio. SUSY events at this point are therefore dominated by final states involving b -jets and pairs of opposite-sign, same-flavor leptons. Missing transverse energy is not used in the analysis at this point.

3.1 Measurement of $M_{\tilde{\chi}_2} - M_{\tilde{\chi}_1}$

Events are selected by requiring:

- A pair of isolated leptons of opposite charge and the same flavor with $p_{T\ell} > 10 \text{ GeV}$ and $|\eta_\ell| < 2.5$;
- At least two jets tagged as b quarks and having $p_t > 15 \text{ GeV}$ and $|\eta| < 2$; a tagging efficiency of 60% is assumed.

The dilepton invariant mass distribution is shown in Figure 8. The dominant Standard Model background is $t\bar{t}$ production, which is quite small because it has smaller color factors and requires two leptonic decays. This background, as well as the combinatorial background from events with two $\tilde{\chi}$ decays, can be eliminated by calculating the subtracted distribution:

$$\left. \frac{d\sigma}{dM} \right|_{\text{sub}} = \left. \frac{d\sigma}{dM} \right|_{e^+e^-} + \left. \frac{d\sigma}{dM} \right|_{\mu^+\mu^-} - \left. \frac{d\sigma}{dM} \right|_{e^+\mu^-} - \left. \frac{d\sigma}{dM} \right|_{e^-\mu^+}.$$

This subtracted mass distribution has a sharp edge at $M_{\ell^+\ell^-} = M_{\tilde{\chi}_2} - M_{\tilde{\chi}_1}$, enabling this mass difference to be measured with great precision. In view of the enormous size of the event sample, the uncertainty on this measurement will be limited by systematic effects. The large sample of $Z \rightarrow \ell^+\ell^-$ decays will be used for calibration both of the mass scale and of the relative e and μ acceptance. The methods employed will be similar to those used by CDF and D0 in their determinations of the W mass [8, 9]. An estimate of 50 MeV for the uncertainty on $M_{\tilde{\chi}_2} - M_{\tilde{\chi}_1}$ should be conservative.

3.2 Gluino and Sbottom Reconstruction

The next step is a reconstruction of the gluino and sbottom masses by combining a dilepton pair near the mass edge with jets. Events are selected that have

- At least two jets, tagged as having a b quark with $p_t > 15 \text{ GeV}$ and $|\eta| < 2$; a tagging efficiency of 60% is assumed;

- A e^+e^- pair with $45 \text{ GeV} < M_{\ell^+\ell^-} < 55 \text{ GeV}$ and no other electrons or a $\mu^+\mu^-$ pair in the same mass range and no other muons in the event.

Since the mass of the lepton pair is near its maximum value, in the rest frame of $\tilde{\chi}_2$ both $\tilde{\chi}_1$ and the $\ell^+\ell^-$ pair are forced to be at rest. The momentum of $\tilde{\chi}_2$ in the laboratory frame is then determined to be

$$\vec{P}_{\tilde{\chi}_2} = \left(1 + M_{\tilde{\chi}_1^0}/M_{\ell^+\ell^-}\right) \vec{P}_{\ell^+\ell^-} .$$

where $M_{\tilde{\chi}_1^0}$ must be assumed (see below). This momentum can be combined with a b -jet to determine $m_{\tilde{b}}$ and a second b -jet to determine $m_{\tilde{g}}$. The b -jet energy and momentum must be corrected for the fact that particles are lost outside the $R = 0.4$ jet cone and for the fact that weak decays produce neutrinos in the jets. In this study, the correction factor was determined using the data generated for LHC Point 5, where the Higgs peak ($h \rightarrow b\bar{b}$) is observable. In practice, techniques similar to those of references [10, 11] would be used at LHC.

Figure 9 shows a scatterplot of $m_{\tilde{g}} - m_{\tilde{b}}$ vs. $m_{\tilde{g}}$. Projections onto the axes, shown in Figures 10 and 11, have clear peaks. The positions of the peaks determine $m_{\tilde{g}} - m_{\tilde{b}}$ and $m_{\tilde{b}}$ assuming that $M_{\tilde{\chi}_1^0}$ is known. Again, statistical errors are small and the dominant errors will be from the determination of the jet energy scale. A careful jet energy calibration has not been performed, so the peaks in Figures. 10 and 11 are displaced slightly from their nominal values of 277.8 and 20.3 GeV. These systematic errors can be estimated from those currently obtained by CDF and D0 in the determination of the top quark mass [10, 11]. The mass difference $m_{\tilde{g}} - m_{\tilde{b}}$ is insensitive to the assumed $\tilde{\chi}_1^0$ mass while the reconstructed sbottom peak moves.

The dependence of the \tilde{b} mass peak on the assumed value of $M_{\tilde{\chi}_1^0}$ is shown in Figure 12, where $M_{\tilde{\chi}_1^0}$ is varied by $\pm 20 \text{ GeV}$ from its nominal value. In making this plot we have required that the mass difference $M(\tilde{\chi}_2^0 bb) - M(\tilde{\chi}_2^0 b)$ be within 15 GeV of the value where its distribution peaks. This cut removes considerable background as can be seen by comparing the peaks in this figure with that in Fig10. We estimate

$$M_{\tilde{b}}(\text{measured}) - M_{\tilde{b}}(\text{true}) = 1.5 \left(M_{\tilde{\chi}_1^0}(\text{assumed}) - M_{\tilde{\chi}_1^0}(\text{true}) \right) \pm 3 \text{ GeV}$$

and

$$M_{\tilde{g}}(\text{measured}) - M_{\tilde{b}}(\text{measured}) = M_{\tilde{g}}(\text{true}) - M_{\tilde{b}}(\text{true}) \pm 2 \text{ GeV}$$

The $\tilde{\chi}_1^0$ mass will be determined by a global fit of the SUSY model to all the measurements; see Section 7.

3.3 Light Squark Reconstruction

Light squarks can also be reconstructed at this point using the decay chain $\tilde{q}_L \rightarrow \tilde{\chi}_2^0 q$, which has a branching ratio of approximately 10%. There is an enormous background from gluino decays to $b\bar{b}$, so events must be rejected if there is a b -jet present. We use the ATLAS b -tagging study (see Figure 3.42 of Ref. [1]). At low luminosity this study implies that a tagging efficiency of 90% for b -jets can be achieved at the price of misidentifying 25% of the light quark jets as b -jets. While this mistag rate is not adequate in the cases where a b -tag

is required, it implies that 90% of the b -quark jets can be vetoed and 75% of the light quark jets accepted by the same cut. This veto prescription is used in this subsection.

Events are selected as follows:

- At least one jet with $p_t > 125$ GeV and $|\eta| < 2$.
- No b -jets with $p_t > 15$ GeV and $|\eta| < 2$; a vetoing efficiency of 90% is assumed and 25% of non b -jets are assumed to be rejected also.
- An e^+e^- pair with $45 \text{ GeV} < M_{\ell^+\ell^-} < 55 \text{ GeV}$ and no other electrons or a $\mu^+\mu^-$ pair in the same mass range and no other muons in the event.

The reconstruction of the momentum of $\tilde{\chi}_2^0$ is performed using the same method as above by selecting events near the endpoint of the dilepton mass distribution. We assume that the SUGRA model is used to infer the mass of $\tilde{\chi}_1^0$ from the $\tilde{\chi}_2^0 - \tilde{\chi}_1^0$ mass difference. Jets of $|\eta| < 2$ and $p_t > 125$ GeV are now combined with the $\tilde{\chi}_2^0$ and the mass distribution is shown in Figure 13. Even with the 90% vetoing efficiency for b -quarks there are a significant number of b -jets remaining in this plot. The contribution from the light squarks is shown as the dashed-histogram. If the vetoing efficiency were raised to 95% approximately one-half of the remaining b -jets are removed and consequently the peak moves to a larger mass. The peak shown has contributions from \tilde{b}_L of mass 278 GeV and the light quarks that have mass around 310 GeV. Charge $-1/3$ and $+2/3$ squarks are separated by about 5 GeV in mass; this contributes to the broadening of the peak. That the peak is real can be seen by estimating the combinatorial background as follows. Events are mixed by taking the $\tilde{\chi}_2^0$ momentum from one event and the jet from another; both events satisfying the same selection criteria. The mass distribution obtained in this way is shown as the hatched distribution in Figure 13. Conservatively, we estimate an error of 20 GeV on the average \tilde{q}_L mass from this method.

3.4 Branching ratio of $\tilde{\chi}_2 \rightarrow \tilde{\chi}_1^0 \ell^+ \ell^-$

By selecting events with four tagged b -jets and either two or four isolated leptons, the product of branching ratios $BR(\chi_2^0 \rightarrow \tilde{\chi}_1^0 \ell^+ \ell^-) \times BR(\tilde{b} \rightarrow b \chi_2^0 X)$ can be determined. There are 150000 events/10 fb⁻¹ with two dilepton pairs and four b -jets. The backgrounds from non supersymmetric sources are negligible, and again therefore the dominant uncertainties are systematic. Using a value of 3% for the uncertainty on the absolute lepton acceptance, we expect that $BR(\chi_2^0 \rightarrow \tilde{\chi}_1^0 e^+ e^-) \times BR(\tilde{b} \rightarrow b \chi_2^0 X)$ can be determined to be $(14.0 \pm 0.5)\%$

3.5 Electroweak Production of Superpartners

At this SUGRA point, sleptons cannot be produced from the decay of strongly interacting sparticles. The production rates are therefore quite small despite the low masses ($m_{\tilde{e}_L} = 215$ GeV, $m_{\tilde{e}_R} = 206$ GeV) as they must be pair produced in Drell-Yan like processes. The heavier charginos and neutralinos are only rarely produced in the decays of gluinos, so again their dominant production mechanism is electroweak. Unlike the case of sleptons, the direct production rate of the lighter charginos and neutralinos is quite large. An attempt has been made to isolate these processes. This is an example of a case where the analysis of a

complete SUSY signal is needed. The signals that we are attempting to extract stand clearly above Standard Model backgrounds, but we face the large background from the production of strongly interacting sparticles. As so few events pass the cuts, we generated separate data samples corresponding to the electroweak production of sparticles and reweighted the events appropriately.

Events are selected that have:

- A three isolated leptons a pair of which have opposite charge and the same flavor with $p_{T\ell} > 10$ GeV and $|\eta| < 2.5$;
- No jets with $p_t > 30$ GeV in $|\eta| < 3.0$.

The jet veto is needed to remove gluino and squark initiated events. These events have jets in the central region arising from the decay products of the sparticles and from final state gluon radiation. These events also have jets, approximately uniform in rapidity, from initial state radiation. This latter source is also present in the direct production of charginos, neutralinos and sleptons. Figure 14 shows the dilepton invariant mass distribution of the two leptons that have opposite charge and the same flavor. The number of *generated* events in this plot is not large, but are sufficient to demonstrate that in 10 fb^{-1} of data there will be sufficient events for a precise measurement. The background events in this plot (corresponding to three generated events) are from $t\bar{t}$ production, the third lepton being from the decay of a b -quark. A stricter jet veto (20 GeV instead of 30 GeV) reduces this background further.

There is an indication of an edge in the mass distribution corresponding to the decay $\tilde{\chi}_2^0 \rightarrow \tilde{\chi}_1^0 \ell^+ \ell^-$. The events in this plot are dominated by the production of $\tilde{\chi}_2^0 \tilde{\chi}_1^\pm$ final states whose contribution is shown as the dotted histogram. If two isolated leptons are required and the same plot made the result is that there are more events. There is now a potential background from Drell-Yan production of dilepton events which must be eliminated by a cut on missing \cancel{E}_T or the angle between the two leptons; the Drell-Yan events are back-to-back while in the SUSY events the leptons arise from $\tilde{\chi}_2^0 \rightarrow \tilde{\chi}_1^0 \ell^+ \ell^-$ and are therefore close in angle. The production rates in these two and three lepton final states can be compared and used to provide a powerful argument concerning the origin of the lepton samples and provide an additional constraint on the model since, as we will demonstrate in section 7, the measurements that have been made using the strong production of sparticles fix the model parameters, resulting in a *prediction* for the rates shown in Figure 14.

In principle, the decay $\tilde{e}_L \rightarrow \tilde{\chi}_2^0 e$ should be reconstructible by selecting with a least 3 isolated leptons, an oppositely charged pair of which have mass between 45 and 55 GeV. The momentum of $\tilde{\chi}_2^0$ is reconstructed as above and then combined with a third lepton to search for a reconstructed \tilde{e}_L . The extraction of this signal is very difficult. The production rate for gauginos provides a serious background that can only be controlled by increasing the number of isolated leptons required. The dominant slepton production process is $\tilde{e}_L + \tilde{\nu}_e$. This can be extracted only by requiring at least *four* isolated leptons from the decay chain

$$\begin{array}{ccc}
 \tilde{\ell}_L^+ & & + \tilde{\nu}_\ell \\
 \downarrow & & \downarrow \\
 \tilde{\chi}_2^0 + \ell^+ & & \tilde{\chi}_1^+ + \ell^- \\
 \downarrow & & \downarrow \\
 \tilde{\chi}_1^0 + \ell^+ + \ell^- & & \tilde{\chi}_1^0 + \ell^+ + \nu
 \end{array}$$

or alternatively from

$$\begin{array}{ccc}
 \tilde{\ell}_L^+ & & + \tilde{\nu}_\ell \\
 \downarrow & & \downarrow \\
 \tilde{\chi}_2^0 + \ell^+ & & \tilde{\chi}_2^0 + \nu \\
 \downarrow & & \downarrow \\
 \tilde{\chi}_1^0 + \ell^+ + \ell^- & & \tilde{\chi}_1^0 + \ell^+ + \ell^-
 \end{array}$$

The dominant decay chain $\tilde{\nu}_\ell \rightarrow \tilde{\chi}_1^+ \ell$, $\tilde{\chi}_1^+ \rightarrow \tilde{\chi}_1^0 + \text{jets}$ is killed by the jet veto requirement. The experiment is only feasible at high luminosity.

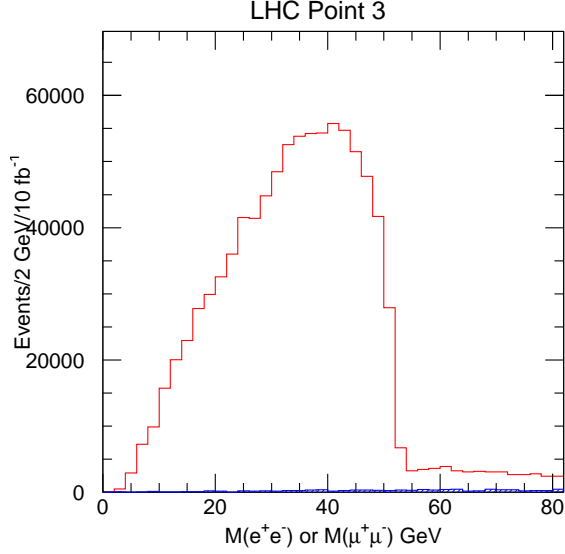


Figure 8: The invariant mass distribution of e^+e^- and $\mu^+\mu^-$ pairs arising at Point 3. The background, shown as a hatched histogram is mainly due to $t\bar{t}$ events.

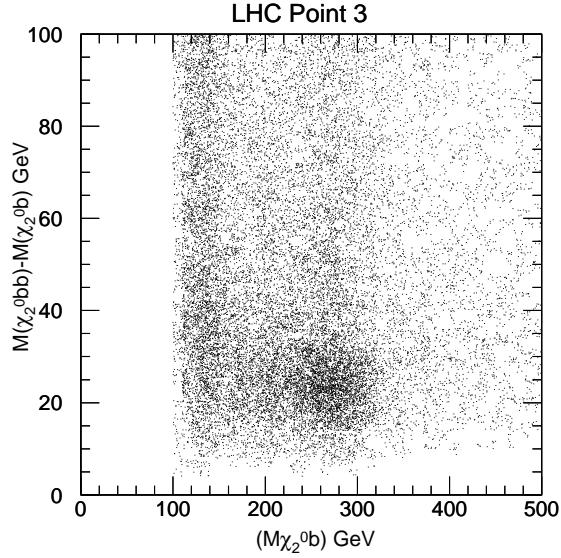


Figure 9: The reconstruction of gluino and sbottom decays from the decay chain $\tilde{g} \rightarrow \tilde{\chi}_2(\rightarrow \tilde{\chi}_1 \ell^+ \ell^-) \tilde{b}$. Events are selected near the endpoint of the $\ell^- \ell^+$ mass distribution (mass between 45 and 55 GeV) and the momentum of $\tilde{\chi}_2$ reconstructed. Two b -jets are then required and the mass of $b + \tilde{\chi}_2$ ($m = m_{\tilde{b}}$) and the mass difference $\delta m = m_{b\tilde{\chi}_2} - m_{b\tilde{\chi}_2}$ is computed. The scatterplot in these two variables is shown. The b -jet energies have been recalibrated and a tagging efficiency of 60% per b included.

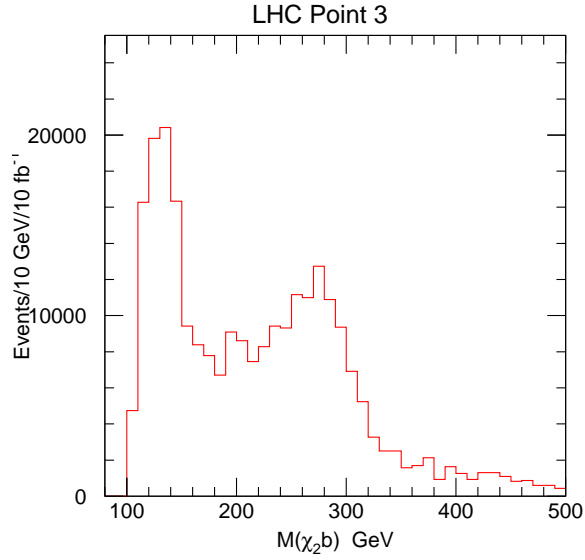


Figure 10: The $M(\tilde{b})$ projection of Figure 9.

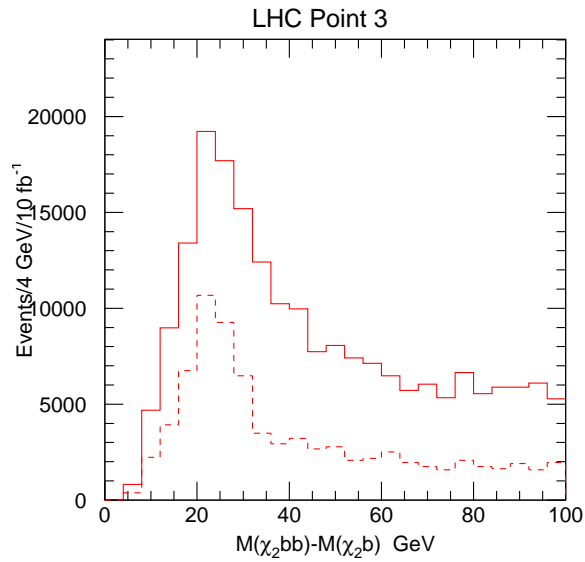


Figure 11: The $M(\tilde{g}) - M(\tilde{b})$ projection of Figure 9. The dashed histogram shows the projection if a cut is made requiring that the events lie in a slice of on the abscissa of between 230 and 330 GeV of Figure 9.

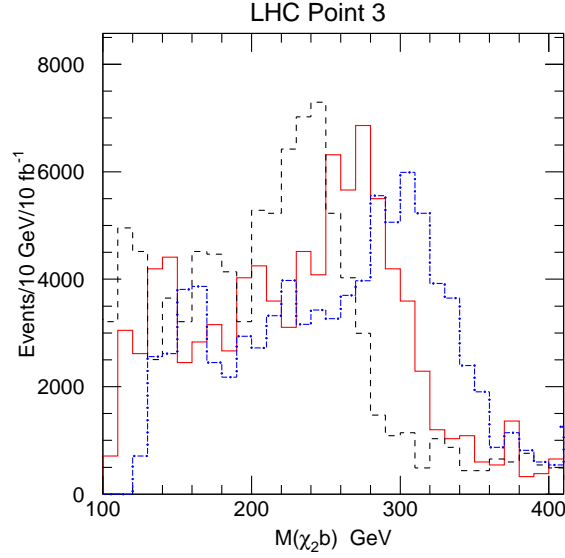


Figure 12: The same as Figure 10 with the addition of two more histograms (dashed and dotted) showing the result if the assumed value of $m_{\tilde{\chi}_1^0}$ is varied by ± 20 GeV. A cut is imposed on the mass difference $|m_{\tilde{g}} - m_{\tilde{b}} - 20| \text{ GeV} < 15 \text{ GeV}$ before the projection of the scatterplots is made.

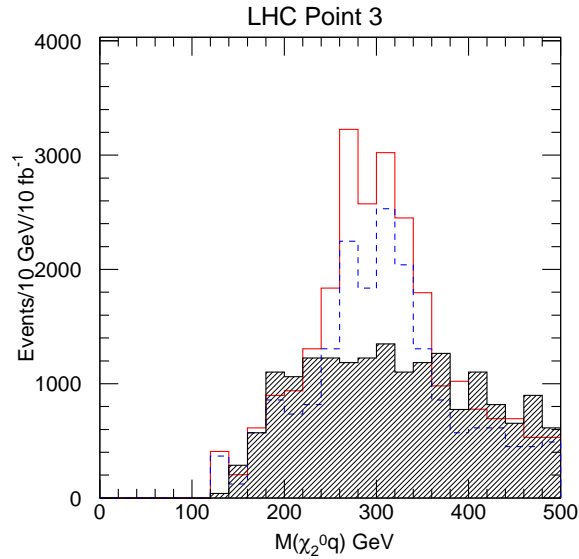


Figure 13: Reconstructed \tilde{q}_L mass at Point 3. The combinatorial background estimate is shown as a hatched histogram and the events due to light squarks as the dashed histogram. The remaining events are due to gluino decays where a b -jet is misidentified as a light quark jet.

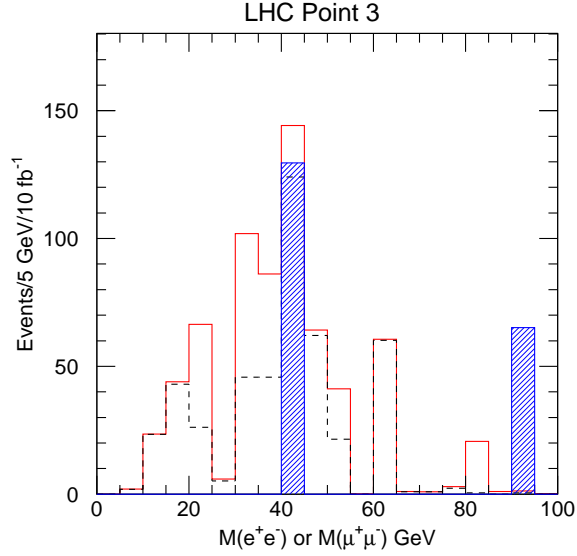


Figure 14: The invariant mass distribution of e^+e^- and $\mu^+\mu^-$ pairs arising at Point 4. Events are selected requiring no jets with $p_t > 30$ GeV in $|\eta| < 3$ and at least three isolated leptons, two of which are of the same flavor and opposite charge. Lepton detection efficiency of 90% per lepton is included. The dashed histogram shows the contribution arising from the direct production of $\tilde{\chi}_1^+ \tilde{\chi}_2^0$ final states. The background is shown as the hatched histogram.

4 LHC Point 4: $m_0 = 800 \text{ GeV}$, $m_{1/2} = 200 \text{ GeV}$, $\tan \beta = 10$

LHC Point 4 has squarks which are much heavier than gluinos, so production of the latter is dominant. The heavier chargino and neutralinos have a much larger admixture of gauginos than at the other points. Hence, the gluinos decay into all combinations of all the charginos and neutralinos and all the quark pairs with comparable branching ratios, giving a very complex mixture of signatures.

4.1 Selection of gaugino decays $\tilde{\chi}_i \rightarrow \tilde{\chi}_j \ell^+ \ell^-$

The objective of this analysis is to isolate opposite-sign, same-flavor dileptons coming from $\tilde{\chi}_2^0 \rightarrow \tilde{\chi}_1^0 \ell^+ \ell^-$, $\tilde{\chi}_{3,4}^0 \rightarrow \tilde{\chi}_1^0 Z$, and $\tilde{\chi}_2^\pm \rightarrow \tilde{\chi}_1^\pm Z$. First, the following cuts were made to suppress the Standard Model backgrounds:

- $M_{\text{eff}} > 800 \text{ GeV}$;
- $\cancel{E}_T > \max(100 \text{ GeV}, 0.15 M_{\text{eff}})$;
- ≥ 4 jets with $p_{T,1} > 100 \text{ GeV}$, $p_{T,2,3,4} > 50 \text{ GeV}$;
- $\ell^+ \ell^-$ pair with $p_{T,\ell} > 10 \text{ GeV}$, $\eta_\ell < 2.5$;
- ℓ isolation cut: $E_T < 10 \text{ GeV}$ in $R = 0.2$;
- Transverse sphericity $S_T > 0.2$.

The opposite-sign, same-flavor and opposite-flavor dilepton mass spectra for the Point 4 signal and the opposite-sign, same-flavor Standard Model background with these cuts are shown in Figure 15. There are clear low-mass and Z opposite-sign, same-flavor signals. (Note that the Z is treated as a narrow resonance in the event generator.) The same-sign Standard Model background is not shown but is smaller than the opposite-sign background.

The difference of the opposite-sign, same-flavor and opposite-sign, opposite-flavor dilepton distributions is shown in Figure 16. This difference should only have contributions from $\tilde{\chi}_2^0 \rightarrow \tilde{\chi}_1^0 \ell^+ \ell^-$ (shown as a dashed curve) and from $Z \rightarrow \ell^+ \ell^-$ decays from heavy charginos and neutralinos, which contribute to the Z peak. Contributions from two independent chargino, top, or W decays contribute equally to both flavor combinations and therefore cancel in this figure. The Standard Model background in the figure fluctuates in sign because of limited statistics but should also mostly cancel.

The edge of the $\tilde{\chi}_2^0 \rightarrow \tilde{\chi}_1^0 \ell^+ \ell^-$ signal is not quite as sharp as in previous cases, but it clearly can be measured with an error of $\sim 1 \text{ GeV}$ or less. The observation both of this edge and of the Z peak shows that both light and heavy gauginos contribute, since for any given gaugino $\tilde{\chi}_i$, decay into $\tilde{\chi}_j Z$ is much larger than decay into $\tilde{\chi}_j \ell^+ \ell^-$.

The relative number of events in the two parts of the distribution can be measured with a statistical error of a few percent. The systematic error on the e and μ acceptance should be comparable to or less than this after Z decays are studied carefully and used for calibration of the calorimeter. Since the sleptons are also heavy at this point, the leptonic branching

ratios for the $\tilde{\chi}_i^0$ are essentially determined by the Z branching ratios, so the relative number of events provides a measure of

$$\frac{\sum_{\tilde{\chi}_i=\tilde{\chi}_{3,4}^0,\tilde{\chi}_2^\pm} B(\tilde{g} \rightarrow \tilde{\chi}_i X) B(\tilde{\chi}_i \rightarrow ZX)}{B(\tilde{g} \rightarrow \tilde{\chi}_2 X)}$$

There are of course non-negligible corrections from squark production and from lepton acceptance.

To see how useful such a branching ratio measurement might be, samples of 10K events each with $m_0 = 800, 700,$ and 600 GeV were generated, forcing the decays $\tilde{\chi}_2^0 \rightarrow \tilde{\chi}_1^0 \ell^+ \ell^-$ and $Z \rightarrow \ell^+ \ell^-$. Figure 17 shows the resulting opposite-sign, same-flavor mass distributions including the 6% leptonic branching ratios. (Subtraction of the same-sign background does not work properly when decays are forced, so the subtracted distribution is not shown.) The number of events in the Z peak and below 70 GeV are 210/2000, 260/2350, and 3000/3150 respectively. The ratio is nearly constant, and the change in absolute number is similar to the change in the total cross section. There is, however, sensitivity to $\tan \beta$, which is more directly related to the mixing of the heavy and light gauginos. A sample of 10K events with $m_0 = 800$ GeV and $\tan \beta = 5$ was generated, again forcing the decays. Figure 18 shows the two distributions; the ratio is 80/1950. More study is needed, but it seems likely that this ratio could constrain $\tan \beta = 10$ to $\sim 10\%$.

The results at this point are very sensitive to the top quark mass. For example, Figure 19 shows the same distribution as Figure 16 for the same SUSY parameters but for $m_t = 170$ GeV instead of 175 GeV. Note that the Z peak is dramatically larger. The reason for this extreme sensitivity is that this point is very close to the boundary of the allowed region: there is no electroweak symmetry breaking for $m_t = 165$ GeV. The possibility of such sensitivity, however, suggests that theoretical uncertainties could play an important role in this region of parameter space.

4.2 Selection of $\tilde{\chi}_4^0 \rightarrow \tilde{\chi}_1^\pm W^\mp \rightarrow e^\pm \mu^\mp X$

Isolated $e\mu$ events come from two independent W or wino decays, not from single Z or neutralino decays. At LHC Point 4 the branching ratio for $\tilde{\chi}_4^0 \rightarrow \tilde{\chi}_1^\pm W^\mp$ is about 84%; this decay contributes to $e^\pm \mu^\mp$ but not to $e^\pm \mu^\pm$. Since the gluino is a Majorana fermion, other channels involving two independent $\tilde{g}\tilde{g}$ or $\tilde{g}\tilde{q}$ decays contribute equally to $e^\pm \mu^\mp$ and $e^\pm \mu^\pm$.

There is a large background to $e^\pm \mu^\mp$ from $t\bar{t}$ production. To suppress this it is necessary to raise the cut on M_{eff} from 800 GeV to 1000 GeV. The like-sign and opposite-sign $e\mu$ mass distributions with this cut and the other cuts described in the previous subsection are shown in Figure 20 together with the Standard Model backgrounds. The difference of the like-sign and opposite-sign distributions is shown in Figure 21. The Standard Model background shows statistical fluctuations but is fairly small after these cuts.

For Point 4 the endpoint of the $e^\pm \mu^\mp$ mass distribution is determined by $\tilde{\chi}_4^0 \rightarrow \tilde{\chi}_1^\pm W^\mp \rightarrow e^\pm \mu^\mp \tilde{\chi}_1^0$ and is 220.6 GeV. This is consistent with Figure 21. Of course other models might lead to the dominance of this decay by other modes. Because there are two missing neutrinos in addition to the $\tilde{\chi}_1^0$, there is no sharp edge at the kinematic limit, so the endpoint can be

determined only roughly. However, the total number of events in Figure 21 can be measured to a few percent; it provides a measure of another combination of branching ratios.

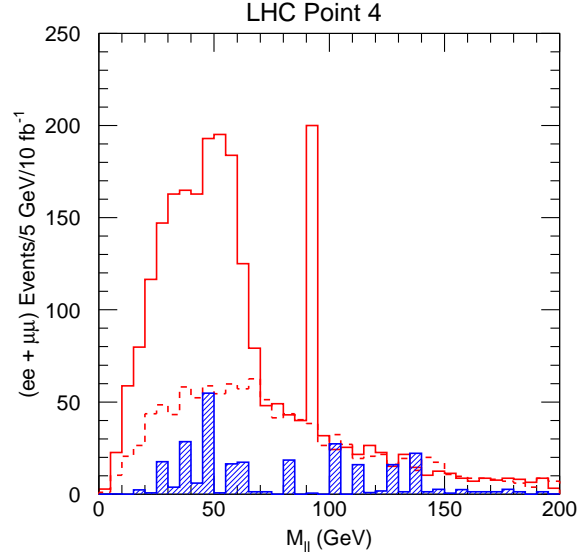


Figure 15: $M_{\ell+\ell^-}$ distribution for opposite-sign, same-flavor dileptons for the Point 4 signal (solid histogram), opposite-sign, opposite-flavor dileptons (dashed histogram), and Standard Model background (shaded histogram).

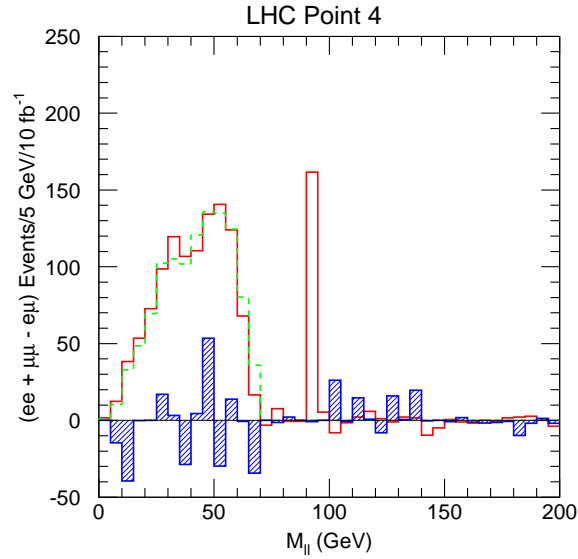


Figure 16: Difference of the $M_{\ell+\ell^-}$ distribution for opposite-sign, same-flavor dileptons and opposite-sign, opposite-flavor dileptons for the Point 4 signal (open histogram) and the Standard Model background (shaded histogram).

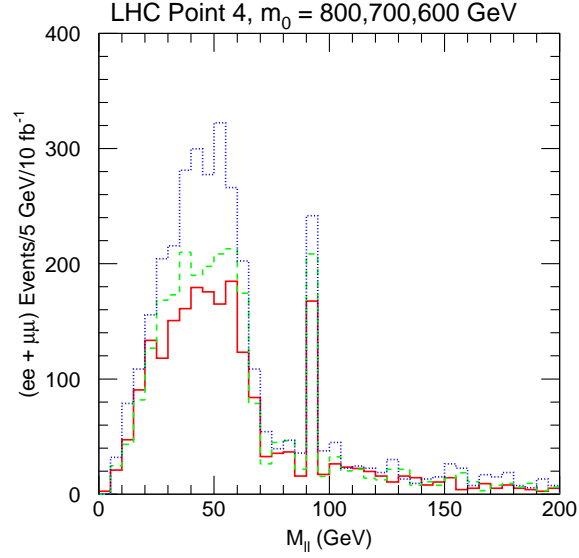


Figure 17: Comparison of $M_{\ell+\ell-}$ distributions for opposite-sign, same-flavor dileptons for $m_0 = 800$ GeV (solid histogram), $m_0 = 700$ GeV (dashed histogram), and $m_0 = 600$ GeV (dotted histogram).

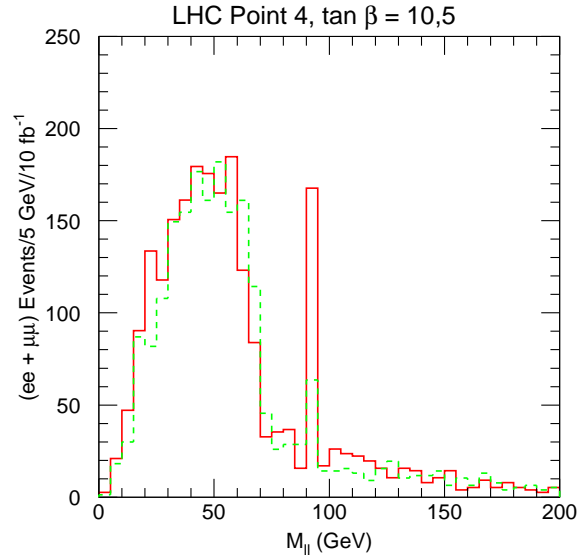


Figure 18: Comparison of $M_{\ell+\ell-}$ distributions for opposite-sign, same-flavor dileptons for $\tan \beta = 10$ (solid histogram) and $\tan \beta = 5$ (dashed histogram).

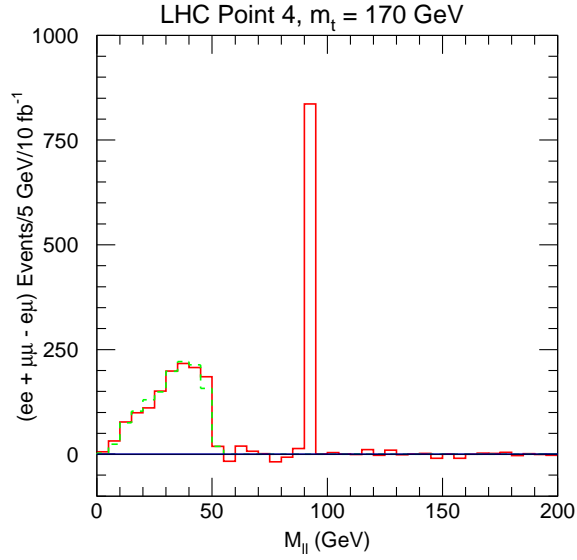


Figure 19: The same as Figure 16 but with $m_t = 170$ GeV. Note the large change in the size of the Z peak.

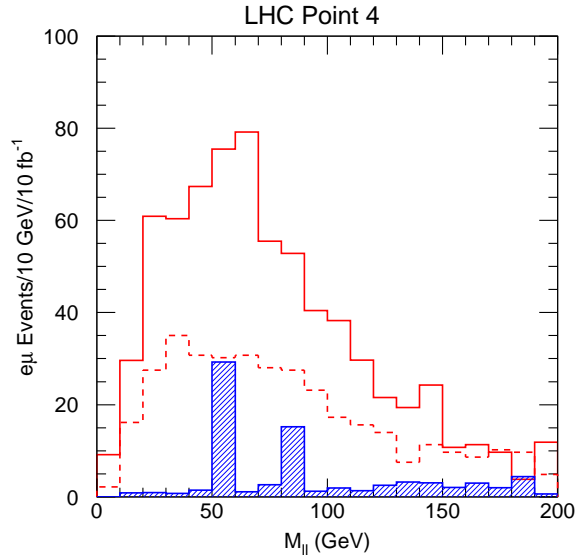


Figure 20: $M_{e^\pm\mu^\mp}$ (solid) and $M_{e^\pm\mu^\pm}$ (dotted) distributions for the Point 4 signal, and Standard Model opposite-sign, opposite-flavor background (shaded histogram).

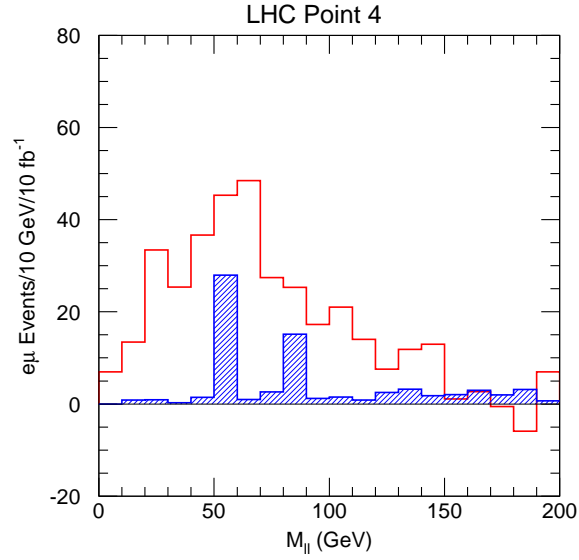


Figure 21: Difference of the $M_{\ell+\ell-}$ distribution for opposite-sign, opposite-flavor and same-sign, opposite-flavor dileptons for the Point 4 signal (open histogram) and the Standard Model background (shaded histogram).

5 LHC Point 5: $m_0 = 100 \text{ GeV}$, $m_{1/2} = 300 \text{ GeV}$, $\tan \beta = 2.1$

LHC Point 5 has a gluino with mass 767 GeV and light squarks with masses of 662–690 GeV, so $\tilde{g} \rightarrow \tilde{q}\bar{q}$ dominates. It has $M(\tilde{\chi}_2^0) = 232.6 \text{ GeV}$, $M(\tilde{\chi}_1^0) = 121.7 \text{ GeV}$, and $M(h) = 104.15 \text{ GeV}$, so $\tilde{\chi}_2^0 \rightarrow \tilde{\chi}_1^0 h$ is kinematically allowed. It also has light right-handed sleptons, $M(\tilde{\ell}_R) = 157.2 \text{ GeV}$, so that $\tilde{\chi}_2^0 \rightarrow \tilde{\ell}_R^\pm \ell^\mp \rightarrow \tilde{\chi}_1^0 \ell^+ \ell^-$ also has a large branching ratio. This point was chosen so that the $\tilde{\chi}_1^0$ provides the correct amount of cold dark matter for cosmology; this generally requires relatively light sleptons [12].

5.1 Selection of $h \rightarrow b\bar{b}$ and Measurement of $M(\tilde{u}_L) - M(\tilde{\chi}_1^0)$

For LHC Point 5 the decay chain $\tilde{\chi}_2^0 \rightarrow \tilde{\chi}_1^0 h$, $h \rightarrow b\bar{b}$ has a large branching ratio, as is typical if this decay is kinematically allowed. The decay $h \rightarrow b\bar{b}$ thus provides a handle for identifying events containing $\tilde{\chi}_2^0$'s [5]. Furthermore, the gluino is heavier than the squarks and so decays into them. The strategy for this analysis is to select events in which one squark decays via

$$\tilde{q} \rightarrow \tilde{\chi}_2^0 q, \tilde{\chi}_2^0 \rightarrow \tilde{\chi}_1^0 h, h \rightarrow b\bar{b},$$

and the other via

$$\tilde{q} \rightarrow \tilde{\chi}_1^0 q,$$

giving two b jets and exactly two additional hard jets.

ISAJET 7.22 [7] was used to generate a sample of 100K events for Point 5, corresponding to about 5.6 fb^{-1} so the signal statistics shown in this section roughly correspond to the actual statistics expected in 1 year at low luminosity. The background samples generally represent a small fraction of an LHC year. The detector response was simulated using the toy calorimeter described above. Jets were found using a fixed cone algorithm with $R = 0.4$. The following cuts were imposed:

- $\cancel{E}_T > 100 \text{ GeV}$;
- ≥ 4 jets with $p_T > 50 \text{ GeV}$ and $p_{T,1} > 100 \text{ GeV}$;
- Transverse sphericity $S_T > 0.2$;
- $M_{\text{eff}} > 800 \text{ GeV}$;
- $\cancel{E}_T > 0.2 M_{\text{eff}}$.

As before, jets were tagged as b 's if they contained a B hadron with $p_T > 5 \text{ GeV}$ and $\eta < 2$, and a tagging efficiency of 60% per b was included.

Figure 22 shows the resulting $b\bar{b}$ mass distributions for the signal and the sum of all Standard Model backgrounds with $p_{T,b} > 25 \text{ GeV}$ together with a Gaussian plus quadratic fit to the signal. The mistagging background is comparable to the real background shown. The energy calorimeter scale for b -jets was recalibrated to bring the Higgs mass peak to its correct value which will be measured ultimately via the decay to $\gamma\gamma$. The correction is about 8%. Using a larger cone, $R = 0.7$, gives an uncorrected peak which is closer to the true mass but wider. Note that for Point 5 the light Higgs could be discovered in this channel with

much less integrated luminosity than is needed to observe $h \rightarrow \gamma\gamma$; the latter would provide a better mass measurement, $\Delta M_h < 1 \text{ GeV}$.

Events were then required to have exactly one $b\bar{b}$ pair with invariant mass within $\pm 1.5\sigma$ ($\sim 19 \text{ GeV}$) of the Higgs peak and exactly two additional jets with $p_T > 75 \text{ GeV}$. The invariant mass of each jet with the $b\bar{b}$ pair was calculated. For the desired decay chain, one of these two must come from the decay of a single squark, so the smaller of them must be less than the kinematic limit for the decay chain $\tilde{q} \rightarrow \tilde{\chi}_2^0 q \rightarrow \tilde{\chi}_1^0 h q$, namely

$$(M_{hq}^{\max})^2 = M_h^2 + (M_{\tilde{q}}^2 - M_{\tilde{\chi}_2^0}^2) \left[\frac{M_{\tilde{\chi}_2^0}^2 + M_h^2 - M_{\tilde{\chi}_1^0}^2 + \sqrt{(M_{\tilde{\chi}_2^0}^2 - M_h^2 - M_{\tilde{\chi}_1^0}^2)^2 - 4M_h^2 M_{\tilde{\chi}_1^0}^2}}{2M_{\tilde{\chi}_2^0}^2} \right].$$

Using the average of the u_L and d_L masses gives $M_{hq}^{\max} = 506 \text{ GeV}$. The smaller of the two $b\bar{b}j$ masses is plotted in Figure 23 for the signal and for the sum of all backgrounds and shows an edge near the expected value. The Standard Model background shows fluctuations from the limited Monte Carlo statistics but seems to be small near the edge, at least for the idealized detector considered here. There is some background from the SUSY events above the edge, presumably from other decay modes and/or initial state radiation.

A detailed understanding of the shape of this edge and its relation to the masses involved requires more study. Based on the statistics in Figure 23, it seems likely that one could determine the end point of the spectrum to $\sim 40 \text{ GeV}$ in one year and to half of that in three years at low luminosity.

5.2 Selection of $W \rightarrow q\bar{q}$ and Measurement of $M(\tilde{u}_L) - M(\tilde{\chi}_1^0)$

Point 5 also has a large combined branching ratio for one gluino to decay via

$$\tilde{g} \rightarrow \tilde{q}_L \bar{q}, \quad \tilde{q}_L \rightarrow \tilde{\chi}_1^\pm q, \quad \tilde{\chi}_1^\pm \rightarrow \tilde{\chi}_1^0 W^\pm, \quad W^\pm \rightarrow q\bar{q},$$

and the other via

$$\tilde{g} \rightarrow \tilde{q}_R q, \quad \tilde{q}_R \rightarrow \tilde{\chi}_1^0 q,$$

giving two hard jets and two softer jets from the W . The branching ratio for $\tilde{q}_L \rightarrow \tilde{\chi}_1^0 q$ is small for Point 5, so the contributions from $\tilde{g} \rightarrow \tilde{q}_L \bar{q}$ and from $\tilde{q}_L \tilde{q}_L$ pair production are suppressed.

The same signal sample was used as in the previous subsection. The combinatorial background for this decay chain is much larger than for the previous one, so harder cuts are needed:

- $\cancel{E}_T > 100 \text{ GeV}$;
- ≥ 4 jets with $p_{T1,2} > 200 \text{ GeV}$, $p_{T3,4} > 50 \text{ GeV}$, and $\eta_{3,4} < 2$;
- Transverse sphericity $S_T > 0.2$;
- $M_{\text{eff}} > 800 \text{ GeV}$;
- $\cancel{E}_T > 0.2 M_{\text{eff}}$.

The same b -tagging algorithm was applied to tag the third and fourth jets as not being b jets. In practice one would measure the b -jet distributions and subtract them.

The mass distribution M_{34} of the third and fourth highest p_T jets with these cuts is shown in Figure 24 for the signal and the sum of all backgrounds. A peak is seen a bit below the W mass with a fitted width smaller than that for the h in Figure 22; note that the W natural width has been neglected in the simulation of the decays.[†] The Standard Model background is more significant here than for the $h \rightarrow b\bar{b}$ channel. Events from this peak can be combined with another jet as was done for $h \rightarrow b\bar{b}$, providing another determination of the squark mass, Figure 25, with an error similar to the previous one. Figure 24 also provides a starting point for measuring the W production rate in SUSY events. Knowing this rate is essential when searching for excess leptons from other sources such as gaugino decays.

5.3 Selection of $\tilde{\chi}_2^0 \rightarrow \tilde{\ell}\ell \rightarrow \tilde{\chi}_1^0\ell\ell$

Point 5 has relatively light sleptons, as is generically necessary if the $\tilde{\chi}_1^0$ is to provide acceptable cold dark matter [12], since $\tilde{\chi}_1^0 - \tilde{\chi}_1^0$ annihilation in the early universe proceeds via slepton exchange and the slepton mass must therefore be small enough to make this rate sufficiently large. Hence the two-body decay

$$\tilde{\chi}_2^0 \rightarrow \tilde{\ell}_R^\pm \ell^\mp \rightarrow \tilde{\chi}_1^0 \ell^+ \ell^-$$

is kinematically allowed and competes with the $\tilde{\chi}_2^0 \rightarrow \tilde{\chi}_1^0 h$ decay, producing opposite-sign, like-flavor dileptons. This source of sleptons is much larger than that from direct production and their discovery is much easier than at Point 3 despite the fact that the total sparticle production rate is much larger at that point. The largest Standard Model background is $t\bar{t}$. To suppress this and other Standard Model backgrounds the following cuts were made on the same signal and Standard Model background samples used previously:

- $M_{\text{eff}} > 800 \text{ GeV}$;
- $\cancel{E}_T > 0.2M_{\text{eff}}$;
- ≥ 1 $R = 0.4$ jet with $p_{T,1} > 100 \text{ GeV}$;
- $\ell^+ \ell^-$ pair with $p_{T,\ell} > 10 \text{ GeV}$, $\eta_\ell < 2.5$;
- ℓ isolation cut: $E_T < 10 \text{ GeV}$ in $R = 0.2$;
- Transverse sphericity $S_T > 0.2$.

With these cuts very little Standard Model background survives, and the $M_{\ell\ell}$ mass distribution shown in Figure 26 has an edge near the kinematic limit for this decay sequence, namely

$$M_{\ell\ell}^{\text{max}} = M_{\tilde{\chi}_2^0} \sqrt{1 - \frac{M_\ell^2}{M_{\tilde{\chi}_2^0}^2}} \sqrt{1 - \frac{M_{\tilde{\chi}_1^0}^2}{M_\ell^2}} \approx 108.6 \text{ GeV},$$

Table 3: Comparison of masses relevant to dilepton spectrum for Point 5 and for modified point with $m_0 = 120$ GeV.

Mass	Point 5	With $m_0 = 120$ GeV
\tilde{g}	767.1 GeV	767.2 GeV
$\tilde{\chi}_2^0$	231.2 GeV	231.4 GeV
$\tilde{\ell}_R$	157.2 GeV	170.6 GeV
$\tilde{\chi}_1^0$	121.3 GeV	121.4 GeV

Observing both $h \rightarrow b\bar{b}$ with $M_h > M_Z$ and an $\ell^+\ell^-$ continuum with $M_{\ell\ell} > M_Z$ would certainly suggest, and perhaps establish, the existence of light sleptons.

If $M_{\ell\ell}$ is near its kinematic limit, then the velocity difference between the $\ell^+\ell^-$ pair and the $\tilde{\chi}_1^0$ is minimized in the rest frame of $\tilde{\chi}_2^0$. Having both leptons hard requires $M_{\tilde{\ell}}/M_{\tilde{\chi}_2^0}^2 \sim M_{\tilde{\chi}_1^0}/M_{\tilde{\ell}}$. Assuming this and $M_{\tilde{\chi}_2^0} = 2M_{\tilde{\chi}_1^0}$ implies that the endpoint in Figure 26 is equal to the $\tilde{\chi}_1^0$ mass. An improved estimate could be made by detailed fitting of all the kinematic distributions. Events were selected with $M_{\ell\ell}^{\max} - 10 \text{ GeV} < M_{\ell\ell} < M_{\ell\ell}^{\max}$, and the $\tilde{\chi}_1^0$ momentum was calculated using this crude $\tilde{\chi}_1^0$ mass and

$$\vec{p}_{\tilde{\chi}_1^0} = (M_{\tilde{\chi}_1^0}/M_{\ell\ell}) \vec{p}_{\ell\ell}.$$

The invariant mass $M_{\ell\ell\tilde{\chi}_1^0}$ of the $\ell^+\ell^-$, the highest p_T jet, and the $\tilde{\chi}_1^0$ was then calculated and is shown in Figure 27. A broad peak is seen near the light squark masses, 660–688 GeV. This peak contains complementary information to that obtained from Figure 23 and more information about the masses could be obtained by performing a combined fit.

A detailed analysis of the dilepton mass spectrum would require varying $M(\tilde{\chi}_2^0)$, $M(\tilde{\ell}_R)$, $M(\tilde{\chi}_1^0)$, and the $p_T(\tilde{\chi}_2^0)$ distribution and fitting the distributions of $M(\ell\ell)$, $p_T(\ell\ell)$, $p_T(h)$, and $p_T(\ell_2)/p_T(\ell_1)$. Rather than do this, a sample of 50K events with $m_0 = 120$ GeV but otherwise the same parameters was generated. A comparison of some of the relevant masses is shown in Table 3; the slepton mass changes by 13 GeV, and the rest are essentially identical. The $M(\ell\ell)$ mass distribution near the edge is shown in Figure 28. There is a shift in the location of the edge by about 2 GeV, which should be observable. There is not much change in the p_T distribution of the $\ell\ell$ pair, Figure 29. The most sensitive distribution is $p_T(\ell_2)/p_T(\ell_1)$, where by definition $p_T(\ell_2) < p_T(\ell_1)$. There is a clear change in the shape, as one would expect. For fixed values of the other parameters, one ought to be able to determine m_0 to ~ 5 GeV, although careful subtraction of Standard Model backgrounds will be necessary.

5.4 Top Production in SUSY Events

Glino decays at LHC Point 5 have a sizable branching ratio to $t\bar{t}$. We have attempted to isolate such a sample by searching for top decays. In order to reduce the background from Standard Model top production, the cut on M_{eff} has been raised to $M_{\text{eff}} > 1000$ GeV for this analysis. The event selection is as follows:

[†]The Higgs width is much smaller than the W width for Higgs masses relevant to these analyses.

- $\cancel{E}_T > 100 \text{ GeV}$;
- ≥ 4 jets with $p_{T1} > 100 \text{ GeV}$, $p_{T2,3,4} > 50 \text{ GeV}$;
- Transverse sphericity $S_T > 0.2$;
- $M_{\text{eff}} > 1000 \text{ GeV}$;
- $\cancel{E}_T > 0.2M_{\text{eff}}$.
- Exactly two b-jets with $p_T > 25 \text{ GeV}$.

If the invariant mass of the two- b system is within $\pm 20 \text{ GeV}$ of the Higgs mass, the event is rejected. To search for $W \rightarrow q\bar{q}$, we calculate the invariant mass of all dijet combinations with both jets having $p_T > 50 \text{ GeV}$ and with neither jet being tagged as a b. Combinations with $|M_{q\bar{q}} - M_W| < 10 \text{ GeV}$ mass are considered W candidates. Combinations where $20 \text{ GeV} < |M_{q\bar{q}} - M_W| < 30 \text{ GeV}$ are used to model the shape of the background; we will refer to these events as the W sideband region. The $M_{q\bar{q}}$ distribution is shown in Figure 31 where a clear W peak is visible. The average jet multiplicity in these events is ~ 9 and hence there is a large combinatorial background in this figure.

Dijets in the W mass and W sideband regions are then combined with each of the two b jets, giving two combinations for each W . Results of this reconstruction for the W signal and sideband regions are shown in Figure 32. Subtraction of the sideband distribution from the signal yields Figure 33. A clear top signal is seen. There is a small background of Standard Model production of top quarks, shown as the hatched histogram on this figure. The dominant decay chain giving rise to this signal is

$$\begin{aligned}\tilde{g} &\rightarrow \tilde{t}t \\ \tilde{t} &\rightarrow \tilde{\chi}_1^+ b \\ \tilde{\chi}_1^+ &\rightarrow \tilde{\chi}_1^0 W\end{aligned}$$

The kinematics of the decay $\tilde{t} \rightarrow \tilde{\chi}_1^+ b$, $\tilde{\chi}_1^+ \rightarrow \tilde{\chi}_1^0 W$ restricts the Wb invariant mass distribution to be between 203 and 356 GeV. There is some evidence in Figure 33 for an excess of events in this region. Unfortunately, other possible combinations and decays such as $\tilde{g} \rightarrow \tilde{b}b$, $\tilde{b} \rightarrow \tilde{\chi}_1^+ t$, $\tilde{\chi}_1^+ \rightarrow \tilde{\chi}_1^0 W$, which has a smaller combined branching fraction, make the exact interpretation difficult. Thus, when discussing the determination of SUSY parameters in Section 7.2, we assume that top decays in SUSY events can be seen at Point 5 (indicating that the $\tilde{g} \rightarrow \tilde{t}t$ channel is open), but we will not assume that the \tilde{t} mass can be determined.

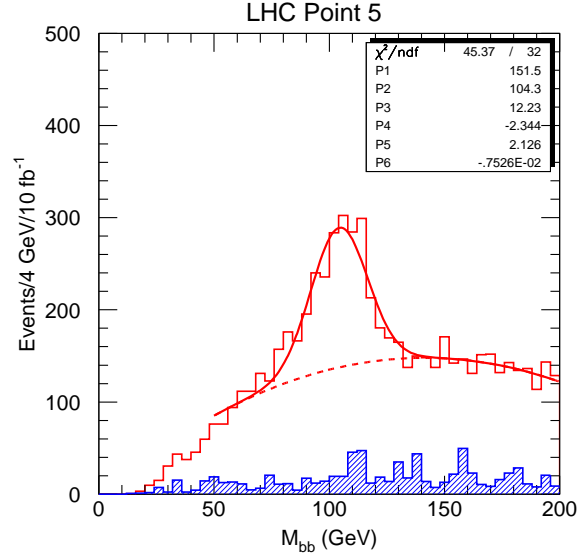


Figure 22: $M(b\bar{b})$ for pairs of b jets for the Point 5 signal (open histogram) and for the sum of all backgrounds (shaded histogram) after cuts described in the text. The smooth curve is a Gaussian plus quadratic fit to the signal. The light Higgs mass is 104.15 GeV.

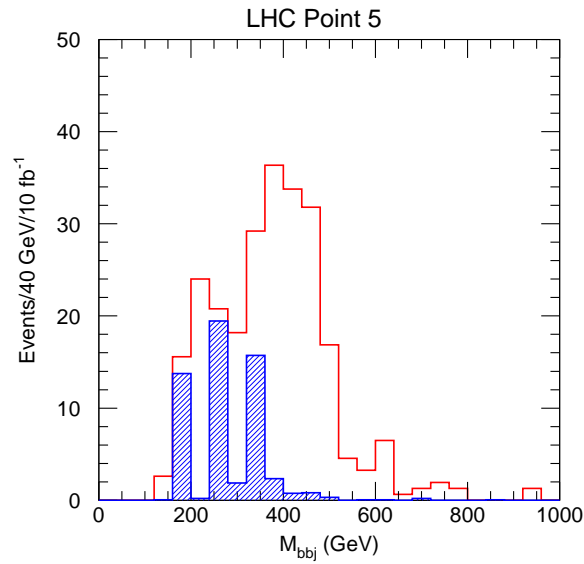


Figure 23: The smaller of the two $b\bar{b}j$ masses for the signal and background events with $73 < M(b\bar{b}) < 111$ GeV in Figure 22 and exactly two additional jets j with $p_T > 75$ GeV. The endpoint of this distribution should be approximately $M_{hq}^{\max} = 506$ GeV.

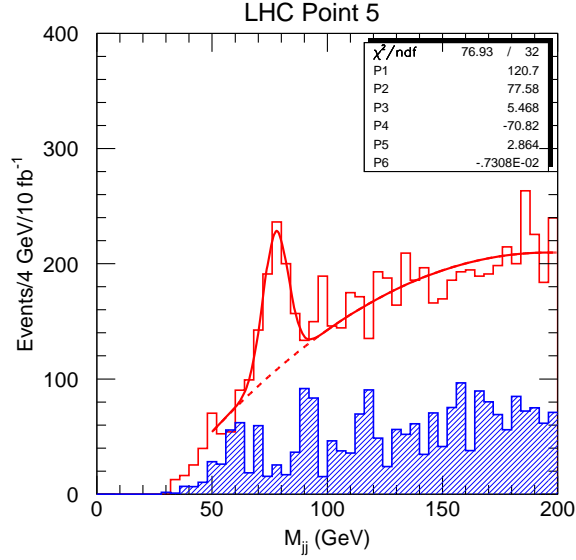


Figure 24: M_{34} for non- b jets in events with two 200 GeV jets and two 50 GeV jets for the Point 5 signal (open histogram) and the sum of all backgrounds (shaded histogram).

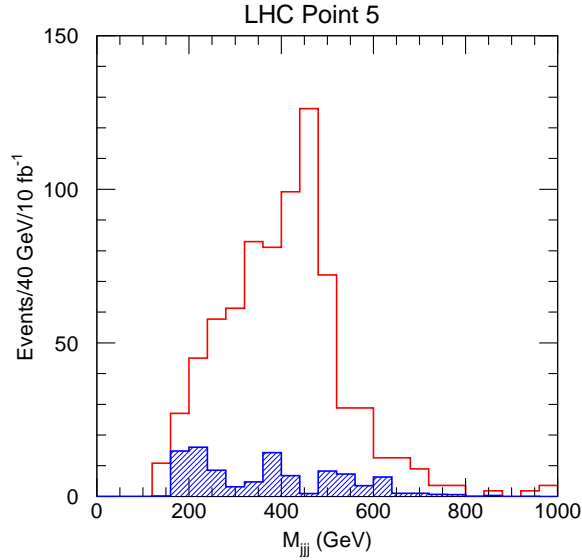


Figure 25: The smaller of the two $q\bar{q}j$ masses for signal and background (shaded) events with $71 < M(b\bar{b}) < 87$ GeV in the previous figure and with exactly two additional jets j with $p_T > 75$ GeV. The endpoint of this distribution should be approximately the mass difference between the squark and the $\tilde{\chi}_1^0$, about 565 GeV.

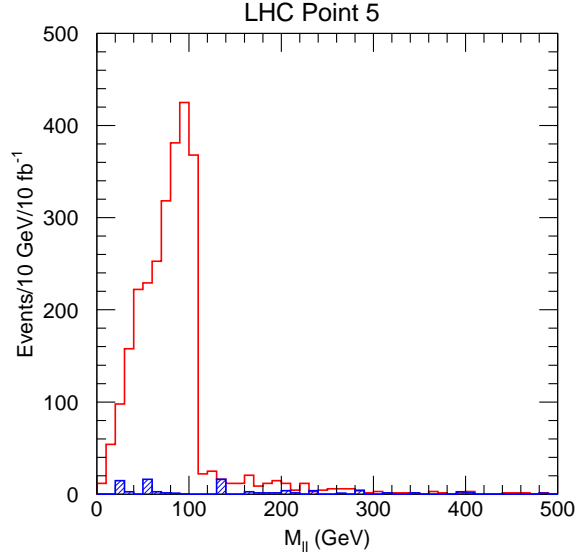


Figure 26: $M_{\ell\ell}$ for the Point 5 signal (open histogram) and the sum of all backgrounds (shaded histogram).

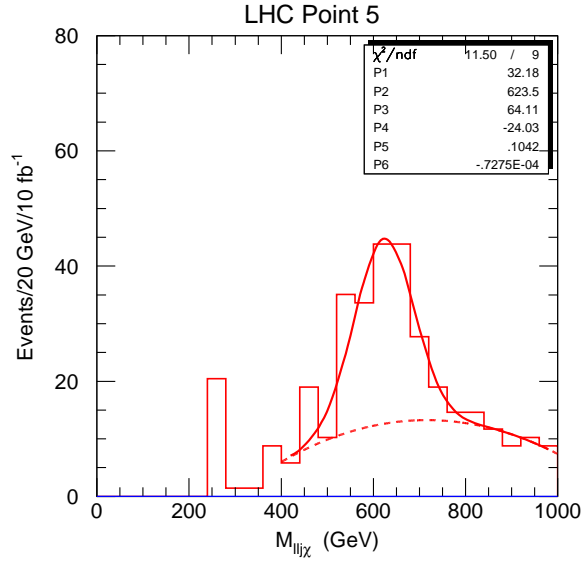


Figure 27: $M_{\ell\ell j\tilde{\chi}_1^0}$ for events with $86 < M_{\ell\ell} < 109$ GeV using $\vec{p}_{\tilde{\chi}_1^0} = M_{\tilde{\chi}_1^0}/M_{\ell\ell}\vec{p}_{\ell\ell}$ for the Point 5 signal (open histogram) and the Standard Model background (shaded histogram).

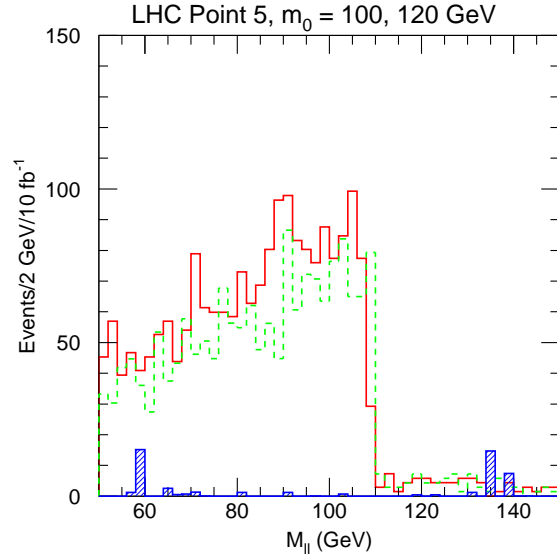


Figure 28: $M(\ell\ell)$ for Point 5 (solid curve) and for a modified point with $m_0 = 120$ GeV (dashed curve). The shaded histogram is the sum of all Standard Model backgrounds.

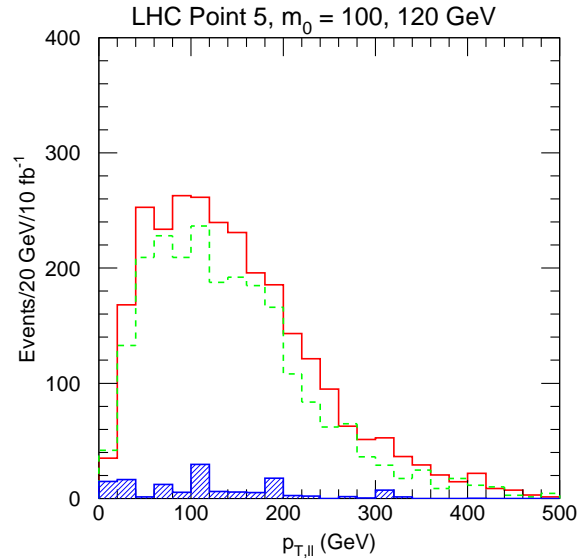


Figure 29: $p_T(\ell\ell)$ for Point 5 (solid curve) and for a modified point with $m_0 = 120$ GeV (dashed curve). The shaded histogram is the sum of all Standard Model backgrounds.

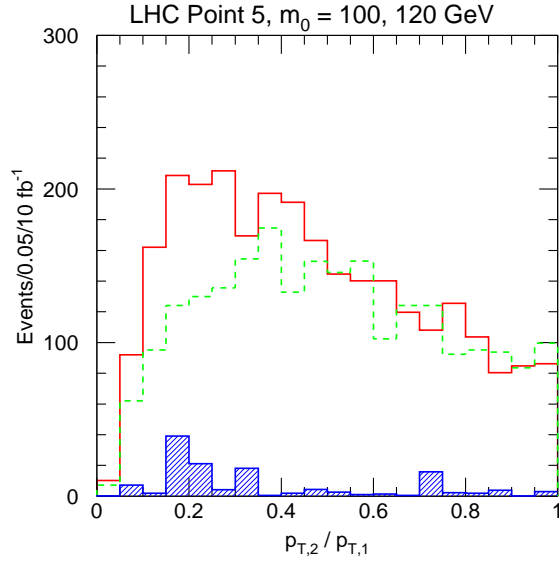


Figure 30: $p_T(\ell_2)/p_T(\ell_1)$ for Point 5 (solid curve) and for a modified point with $m_0 = 120$ GeV (dashed curve). The shaded histogram shows the sum of all backgrounds.

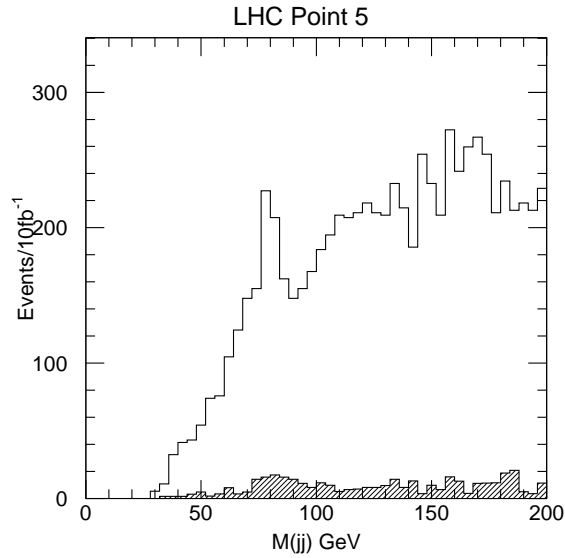


Figure 31: The invariant mass distribution used to search for $W \rightarrow q\bar{q}$ decays in the Point 5 top reconstruction. The shaded histogram shows the sum of all backgrounds.

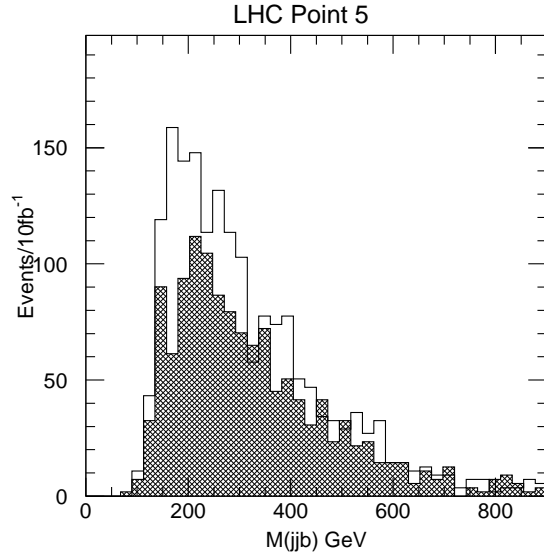


Figure 32: The invariant mass distribution of $q\bar{q}b$ candidates for combinations where the $q\bar{q}$ pair are in the W mass region (solid) and W sideband region (dashed). The b -jet energies have **not** been recalibrated and a tagging efficiency of 60% per b included. Note that each event appears twice.

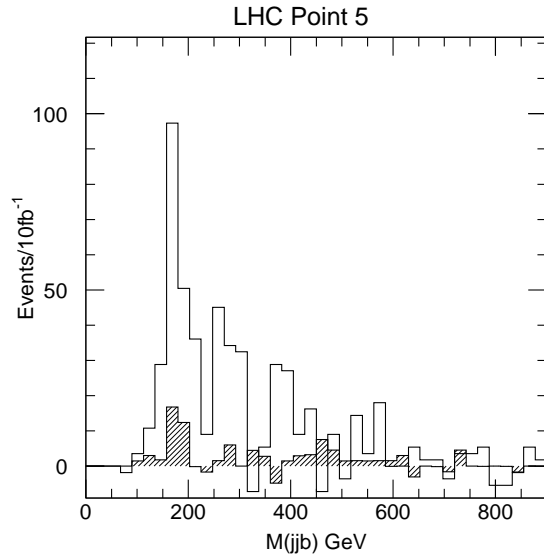


Figure 33: The sideband subtracted invariant mass distribution of Wb candidates. The hatched distribution shows the contribution from Standard Model production of top quarks.

6 LHC Points 1, 2: $m_0 = m_{1/2} = 400$ GeV, $\tan \beta = 2, 10$

LHC Points 1 and 2 have gluino masses of about 1 TeV and squark masses about 50 GeV lighter. These are close to the upper limit of the expected range if SUSY is to be relevant to electroweak symmetry breaking. The cross sections are quite small, so more than 10 fb^{-1} is needed for precision studies. Only a few results will be presented here.

6.1 Selection of $h \rightarrow b\bar{b}$ and Measurement of $M(\tilde{u}_L) - M(\tilde{\chi}_1^0)$

This analysis is very similar to the one for LHC Point 5, but since the signal cross sections are smaller, harder cuts are needed:

- $\cancel{E}_T > 100$ GeV;
- ≥ 4 jets with $p_T > 50$ GeV, $p_{T,1} > 250$ GeV $p_{T,2} > 150$ GeV;
- Transverse sphericity $S_T > 0.2$;
- $M_{\text{eff}} > 1000$ GeV;
- $\cancel{E}_T > 0.2M_{\text{eff}}$.

Events with exactly two tagged b jets were then selected. Figures 34 and 35 show the $b\bar{b}$ mass distributions for Points 1 and 2 respectively. The light Higgs would be discovered in this mode at either point with 10 fb^{-1} or less, although $h \rightarrow \gamma\gamma$ would still be needed to provide the most precise mass determination.

Events passing these cuts and having a $b\bar{b}$ mass within 2σ of the peak were then selected. These events were also required to have two and only two additional jets with $p_T > 100$ GeV. This cut is quite inefficient, but attempts to improve its efficiency produced more background. Each of the two jets was combined with the $b\bar{b}$ pair. The smaller of the two masses was selected for each event and plotted in Figures.36 and 37. The endpoints for the decay sequence $\tilde{q}_L \rightarrow \tilde{\chi}_2^0 q \rightarrow \tilde{\chi}_1^0 b\bar{b}q$ are 739 GeV and 751 GeV respectively. Measurement of this edge will be limited by statistics to ~ 50 GeV for 10 fb^{-1} .

6.2 Selection of $\tilde{\chi}_i \rightarrow \tilde{\chi}_j \ell^+ \ell^-$

Sleptons are quite heavy for LHC Points 1 and 2, so there is no edge in the dilepton mass spectrum as for Point 5. There is, however, a $Z \rightarrow \ell^+ \ell^-$ signal that can be used to distinguish these otherwise rather similar points.

The basic selection cuts given at the beginning of the previous subsection were applied. In addition, the events were required to have two opposite-sign, same-flavor leptons with $p_T > 10$ GeV, $|\eta| < 2.5$, and $E_T < 10$ GeV in a cone $R = 0.2$. The mass of the two highest p_T such leptons is shown in Figure 38 and Figure 39 for LHC Points 1 and 2 respectively. The Z peak is questionable for Point 1 but rather clear for Point 2, which has larger $\tan \beta$ and hence more mixing of gauginos and Higgsinos. Even for Point 2, however, the statistical error on the number of Z 's is $\sim 15\%$. Clearly this is a measurement that needs higher luminosity.

There are also observable signals in the like-sign and in the opposite-sign, opposite-flavor dilepton channels. These would certainly be useful in a global fit, but they do not seem to provide the sort of precise measurements being considered in this paper.

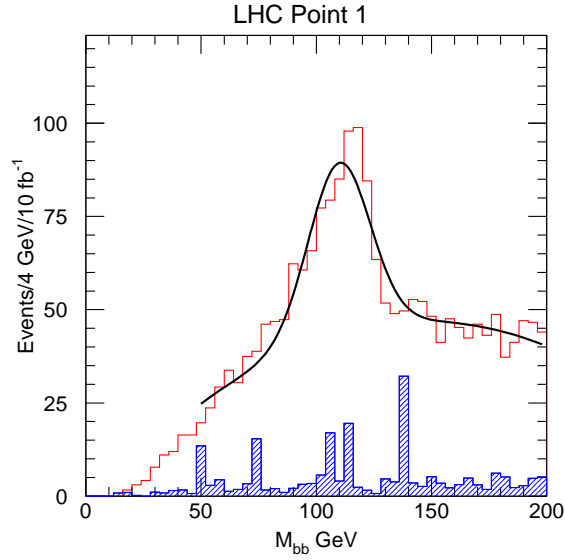


Figure 34: $M(b\bar{b})$ for pairs of b jets for the LHC Point 1 signal (open histogram) and for the sum of all backgrounds (shaded histogram) after cuts described in the text. The smooth curve is a Gaussian plus quadratic fit to the signal. The light Higgs mass is 111.2 GeV.

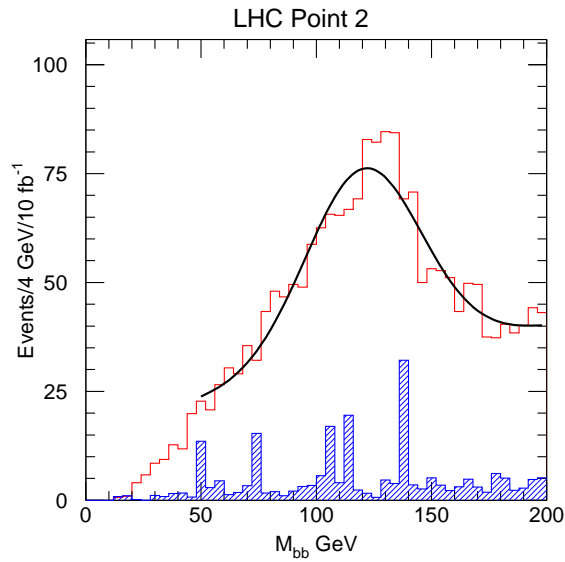


Figure 35: Same as Figure 34 for LHC Point 2. The light Higgs mass is 125.1 GeV.

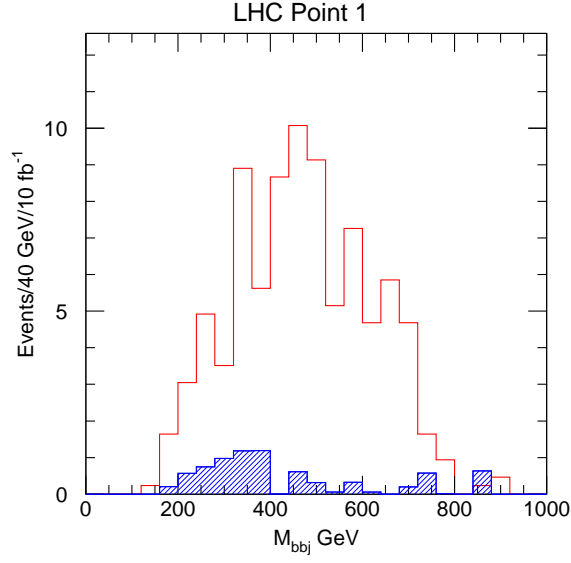


Figure 36: The smaller of the two $b\bar{b}j$ masses for the signal and background events with $M(b\bar{b})$ within 2σ of the peak in Figure 34 and exactly two additional jets j with $p_T > 100$ GeV. The endpoint of this distribution should be approximately $M_{hq}^{\max} = 739$ GeV.

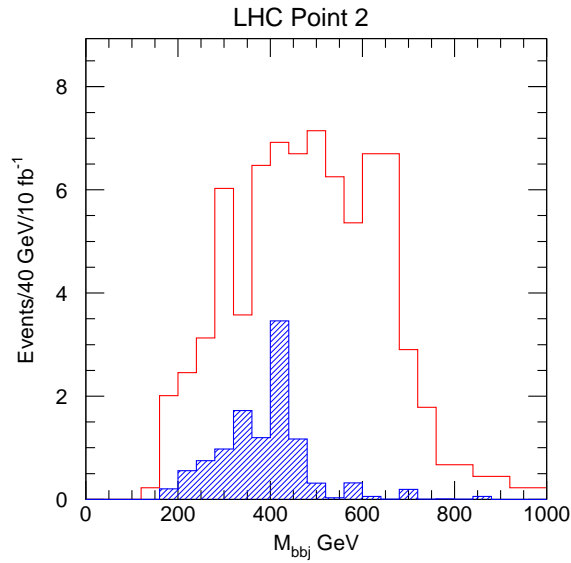


Figure 37: Same as Figure 34 for LHC Point 2. The endpoint should be $M_{hq}^{\max} = 751$ GeV.

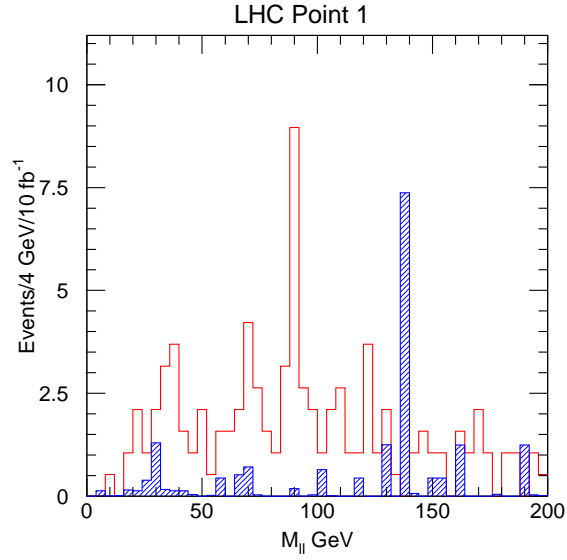


Figure 38: $M_{\ell\ell}$ for the Point 1 signal (open histogram) and the sum of all backgrounds (shaded histogram).

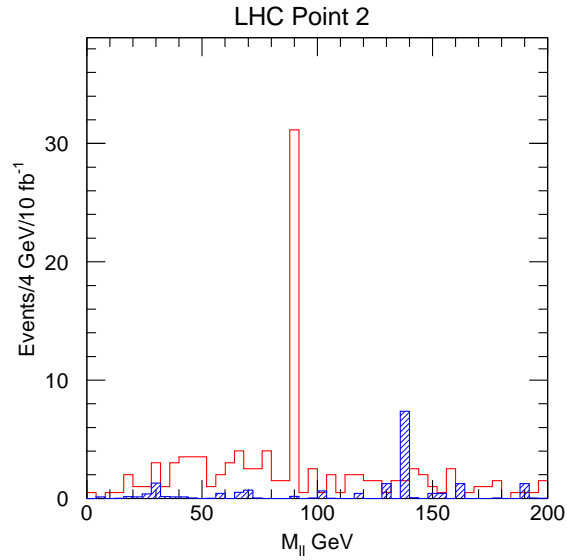


Figure 39: $M_{\ell\ell}$ for the Point 2 signal (open histogram) and the sum of all backgrounds (shaded histogram).

7 Determining SUSY parameters

Once a number of quantities have been measured, we can attempt to determine the particular SUSY model and the values of the parameters. The strategy will be to attempt to perform a global fit to the model parameters using all of the available data, much as the Standard Model is tested using the W and Z masses and the many quantities precisely measured by LEP/SLC. Such a fit is beyond the scope of our work, and we adopt a simpler procedure. We assume that from measurements of global parameters such as those discussed in section 2 we know the approximate scale of the superpartner masses and have some idea that we might be in a SUGRA model. The object is then to determine the parameters of that model and check its consistency. We must therefore determine the parameters m_0 , $m_{1/2}$, A_0 , $\tan\beta$ and $\text{sgn}\mu$. As we will see A_0 is difficult to determine. Its value is given at the unification scale, and the value that is relevant for the phenomenology is the one evolved down to the electroweak scale. Many choices of A_0 evolve to the same (fixed point) value, so there is reduced sensitivity to its value at the unification scale. In addition it always appears scaled by the Yukawa coupling for the relevant quark or lepton. Hence its effect on lepton masses and on the quarks of the first two generations is very small. Its effect is significant for top squarks and at large $\tan\beta$ for bottom squarks. [‡]

Our strategy for determining the parameters is as follows. We choose a point randomly in parameter space and compute the spectrum. We assign a probability to this point determined from how well it agrees with our “measured quantities” using our estimates of the errors on those quantities. The process is repeated for many points and the probabilities used to determine the central values of the parameters, their errors and their correlations. The probability distribution functions are not always Gaussian; the $+1\sigma$ (-1σ) errors quoted below are such that 15.87% of this distribution is below (above) the quoted value. Thus, 68.27% of the probability falls within our definition of $\pm 1\sigma$.

7.1 LHC Point 3

At LHC Point 3 ($m_0 = 200$ GeV, $m_{1/2} = 100$ GeV), LEP will discover h and measure its mass. The relevant error is that from theoretical calculations of the mass in the supergravity model which is likely to dominate the error from the LEP measurement. We will assume an error of ± 3 GeV. Using the results presented in Section 3, we assume the following measurements and errors:

- $M_{\tilde{\chi}_2^0} - M_{\tilde{\chi}_1^0} = 52.36 \pm 0.05$ GeV,
- $M_{\tilde{g}} - M_{\tilde{b}} = 20.3 \pm 2.0$ GeV,
- $M_h = 68.3 \pm 3$ GeV.

As described above the mass difference $M_{\tilde{g}} - M_{\tilde{b}}$ is insensitive to the mass assumed for $\tilde{\chi}_1^0$.

Using the strategy outlined above we get the following constraint on the parameters:

[‡]The Higgs mass that we use is that determined from 1-loop calculations as implemented in ISAJET [7]. Two loop corrections to the Higgs mass, implemented, for example, in SPTHYIA [13] lower the mass by about 5%.

- $m_0 = 200_{-8}^{+13}$ GeV,
- $m_{1/2} = 99.9 \pm 0.7$ GeV,
- $\tan \beta = 1.99 \pm 0.05$,
- the sign of μ is determined to be -1 ,
- A_0 is constrained to be greater than -400 GeV.

There are no clear correlations between the parameters. The additional constraint that the average value of the light squark mass is within ± 20 GeV provides no additional restriction on the parameters. The relevant phenomenological parameter is the value of A evolved down to the electroweak scale. The relevant values are those for the third generation, A_b and A_t . Information on these can only come directly from data on bottom and top squarks. In this case $A_t = -176 \pm 22$ GeV. A_b is not well constrained; it is allowed to range from 50 to -500 GeV. Over this range the mass of the two stop eigenstates varies only slightly from 270 and 320 GeV at one end to 260 and 330 GeV at the other. Constraining A_b is very challenging as it appears scaled by the small factor of the bottom quark Yukawa coupling.

The degree of precision may be surprising. Over most of the SUGRA parameter space $\tilde{\chi}_2^0$ and $\tilde{\chi}_1^0$ are gauginos (*i.e.*, they have no Higgsino components), $M_{\tilde{\chi}_2^0} - M_{\tilde{\chi}_1^0}$ then determines $m_{1/2}$. $M_{\tilde{g}}$ and $M_{\tilde{\chi}_1^0}$ are then predicted and a consistency check of the model made by the measurement of $M_{\tilde{g}}$. Information on m_0 , is then obtained from $M_{\tilde{g}}$ and the value of M_h is sufficient to constrain $\tan \beta$.

The other measurements available at this point are now used to provide powerful consistency checks of the model. The measurement of the bottom squark and other squark masses and the event rates for isolated leptons without jets discussed in Section 3 are examples. Another example is the branching ratio for $\tilde{\chi}_2^0 \rightarrow \tilde{\chi}_1^0 \ell^+ \ell^-$. Figure 40 shows this branching fraction for a selection of SUGRA models that have parameters in the slightly larger range $m_0 = 200 \pm 15$ GeV, $m_{1/2} = 100. \pm 1.5$ GeV, $\tan \beta = 2.0 \pm 0.1$. At Point 3 $BR(\tilde{\chi}_2^0 \rightarrow \tilde{\chi}_1^0 e^+ e^-) = 16.5\%$. This branching ratio can be constrained using the method described in section 3.4;

7.2 LHC Point 5

At LHC Point 5 ($m_0 = 100$ GeV, $m_{1/2} = 300$ GeV, $\tan \beta = 2.1$), h will be discovered at LHC in its decay to $b\bar{b}$ from its production in the decays of supersymmetric particles, and its mass will be measured precisely from its decay to $\gamma\gamma$. Using the results presented in Section 5, we assume the following set of measurements:

- $M_{\tilde{\chi}_2^0} \sqrt{1 - M_t^2/M_{\tilde{\chi}_1^0}^2} \sqrt{1 - M_{\tilde{\chi}_1^0}^2/M_t^2} = 108.6 \pm 1$ GeV,
- The decay $\tilde{g} \rightarrow t\bar{t}$ is allowed,
- The end point of the spectrum in Figure 23 is 506 ± 40 GeV,
- $M_h = 104.15 \pm 3$ GeV.

These results correspond to two possible solutions:

- $m_0 = 100.5_{-8}^{+12}$ GeV,
- $m_{1/2} = 298_{-9}^{+16}$ GeV,
- $\tan \beta = 1.8_{-0.5}^{+0.3}$,
- $\mu = +1$;

and

- $m_0 = 91 \pm 3$ GeV,
- $m_{1/2} = 288 \pm 18$ GeV,
- $\tan \beta = 3.1 \pm 0.2$,
- $\mu = -1$.

Both of these solutions provide good fits to the “data”. While there is no constraint on A , the values of A_t and A_b are constrained: $A_b = -740 \pm 180$ ($A_b = -750 \pm 220$) GeV and $A_t = -495 \pm 30$ ($A_t = -536 \pm 56$) GeV for μ positive (negative). The main differences between the mass spectra for these two solutions are in the masses of χ_2^0 , χ_3^0 , χ_4^0 , and χ_2^\pm and the masses of the heavier Higgs bosons; they are significantly larger in the positive μ case. The claimed sensitivity to the lepton decay spectrum (see Figure 30) of $\delta m_0 \sim 5$ GeV implies that this parameter’s range can be narrowed somewhat. We have not investigated the sensitivity of this spectrum to the sign of μ . At this point the errors used (except for the one on M_h) are limited by statistics, so additional luminosity will cause the errors to drop. Using 0.6 GeV for the error on the dilepton endpoint and 23 GeV for the error on the endpoint of Figure 23 reduces the errors on $m_{1/2}$ and m_0 to ± 7 and ± 9 (± 2.5 and ± 10) respectively for positive (negative) μ ; the error on $\tan \beta$ is not reduced.

As well as the differences in the masses of the heavier Higgs and gauginos noted above, the negative sign solution has larger stop masses and hence a smaller branching ratio for $\tilde{g} \rightarrow \tilde{t}_1 \bar{t}$. We have investigated the sensitivity of the top quark signal discussed in section 5.4 to the sign of μ . The parameters $m_0 = 90.4$ GeV, $m_{1/2} = 290$ GeV, $\tan \beta = 3.1$, $\mu = -1$, and $A = 66$ GeV have the opposite sign of μ from Point 5 but give an excellent fit to the “data” used for fitting at this point.[§] A sample of 100K events was generated for this parameter set, and the analysis leading to Figure 33 was repeated. The result is shown in Figure 41; note that the bins in this figure are twice as wide as those in Figure 33. It can be clearly seen that the amount of reconstructed top in SUSY events is reduced relative to that at Point 5 and that this fact can be used to eliminate this alternative solution. In addition, the solutions with $\mu = -1$ have smaller branching ratios of $\tilde{q} \rightarrow q \tilde{\chi}_1^0 h$ so the observed number of higgs events should be able to severely constrain this case.

[§]This modified point has a combined probability of 98% of fitting the data.

7.3 LHC Point 4

At LHC Point 4 ($m_0 = 800 \text{ GeV}$, $m_{1/2} = 200 \text{ GeV}$, $\tan\beta = 10$), determination of the parameters cannot be done by the simple method already described. Here only two masses can be measured in a straightforward manner; the light Higgs mass from its decay to $\gamma\gamma$ and the $\tilde{\chi}_1^0 - \tilde{\chi}_2^0$ mass difference from the endpoint in the dilepton mass distribution. We use these two measurements and the determination of the SUSY scale from the M_{eff} analysis of Section 2:

- $M_{\tilde{\chi}_2^0} - M_{\tilde{\chi}_1^0} = 69 \pm 1$,
- $M_h = 117.4 \pm 3 \text{ GeV}$,
- $\min(M_{\tilde{g}}, M_{\tilde{u}_R}) = 580 \pm 60 \text{ GeV}$ from the M_{eff} analysis.

These constraints restrict the parameter space to two regions:

- $m_0 = 784_{-262}^{+203} \text{ GeV}$,
- $m_{1/2} = 200 \pm 8 \text{ GeV}$,
- $\tan\beta = 9 \pm 2$,
- A is not constrained,
- $\mu = +1$,
- $A_b < 200 \text{ GeV}$ and $A_t < -150 \text{ GeV}$;

or

- $\tan\beta = 14 \pm 4$,
- $m_0 = 950 \pm 210$,
- $m_{1/2} = 185 \pm 10 \text{ GeV}$,
- A is not constrained,
- $\mu = -1$
- $A_b = -160 \pm 150 \text{ GeV}$ and $A_t = -400 \pm 100 \text{ GeV}$.

The uncertainty on $M_{\tilde{\chi}_2^0} - M_{\tilde{\chi}_1^0}$ is limited by statistics at low luminosity. A reduction in its error would reduce the error on $m_{1/2}$.

In order to constrain parameters further, models whose parameters are consistent with these values would need to be generated and their predictions for the distributions shown in Figures 17, 20, and 21 calculated. Those which are inconsistent with the ‘‘observed’’ distribution can then be rejected. This exercise is beyond the scope of this paper.

7.4 LHC Points 1 and 2

At LHC Point 1 and 2 ($m_0 = 400$ GeV, $m_{1/2} = 400$ GeV, $\tan\beta = 2, 10$), event rates are low and precision measurements difficult at low luminosity. We use the following constraints.

- $M_h = 111.4 \pm 3$ GeV for Point 1, or
- $M_h = 125.4 \pm 3$ GeV for Point 2,
- $\min(M_{\tilde{g}}, M_{\tilde{u}_R}) = 920 \pm 90$ GeV from the M_{eff} ,
- The end point of the spectrum in Figure 23 is 745 ± 50 GeV.

In the case of Point 1, there are two solutions:

- m_0 unconstrained,
- $m_{1/2} = 400_{-50}^{+40}$ GeV,
- $\tan\beta = 2.0_{-0.5}^{+0.4}$,
- $\mu = +1$,
- A is not constrained,
- $A_b = -1100 \pm 200$ GeV and $A_t = -650 \pm 55$ GeV;

and one with negative μ that has instead

- $m_{1/2} = 392_{-50}^{+40}$ GeV,
- $\tan\beta = 3.3_{-0.4}^{+0.5}$.

In the case of Point 2, there is again a solution for either sign of μ :

- m_0 unconstrained,
- $m_{1/2} = 405_{-37}^{+32}$ GeV,
- $\tan\beta = 10.6 \pm 0.3$,
- $\mu = \pm 1$,
- A is not constrained,
- $A_b = -1100 \pm 200$ GeV and $A_t = -800 \pm 55$ GeV.

The lack of a constraint on m_0 at these points is alarming but can be explained. $m_{1/2}$ is large and the renormalization group scaling from the GUT scale forces the squark masses to be comparable to the gluino mass almost independent of the input value of m_0 . In cases of this type one needs to measure slepton masses which are less affected since their renormalization group scaling is controlled by α_{weak} rather than α_s . Since the slepton masses are of order 500 GeV, this is a difficult task. Even a lower bound on the masses would constrain m_0 .

If we reduce the error on the end point of the spectrum in Figure 23 to 20 GeV which might be achievable with high luminosity running at LHC, the uncertainty on $m_{1/2}$ reduces to ± 30 GeV. As in the case of Point 5, the decay $\tilde{g} \rightarrow \tilde{t}t$ is allowed. An analysis similar to that discussed there should be able to establish that this channel is open.

In the case of these points, the negative μ solution can be eliminated. The branching ratio for $\tilde{\chi}_2^0 \rightarrow \tilde{\chi}_1^0 Z$ is shown in Figure 42 as a function of $\tan \beta$ for both signs of μ for the solutions in the allowed range. It can be seen from this Figure that the branching ratio is substantially larger for $\mu = -1$. The decay chain $\tilde{q}_L \rightarrow q\tilde{\chi}_2^0 \rightarrow qZ\tilde{\chi}_1^0$ leads to a small Z peak as shown in Figure 38 which corresponds to $BR(\tilde{\chi}_2^0 \rightarrow \tilde{\chi}_1^0 Z) = 0.6\%$. The smallest branching ratio for the $\mu = -1$ solution shown in Figure 42 is 5.7%, approximately a factor of ten larger. It is clear that these two cases can be distinguished in 10fb^{-1} despite the fact that a larger data set may be required to measure the size of the peak shown in Figure 38. In the case of Point 2, The difference in branching ratios is even greater, again enabling elimination of the $\mu = -1$ solution.

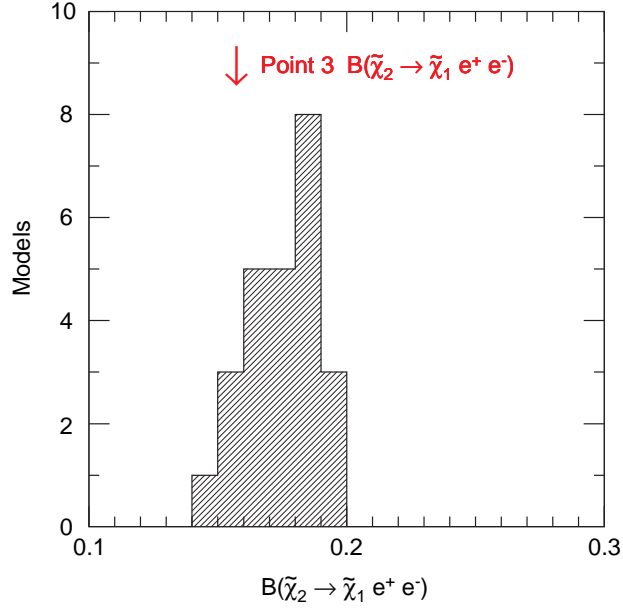


Figure 40: Branching ratio $\tilde{\chi}_2^0 \rightarrow \tilde{\chi}_1^0 \ell^+ \ell^-$ for the SUGRA models $m_0 = 200 \pm 15$ GeV, $m_{1/2} = 100 \pm 1.5$ GeV, $\tan \beta = 2.0 \pm 0.1$.

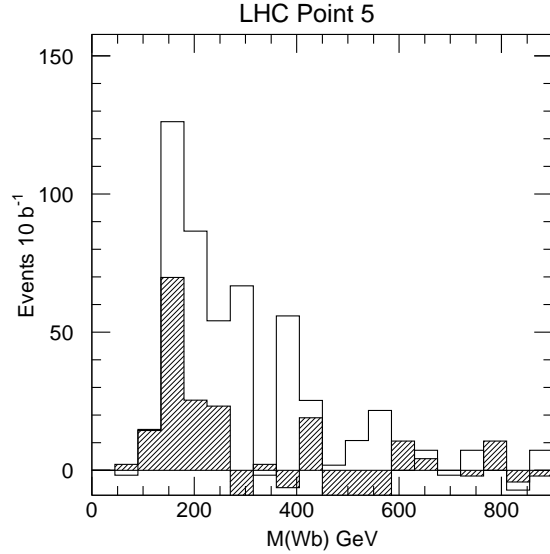


Figure 41: The sideband subtracted invariant mass distribution of Wb candidates. The analysis is as described in section 5.4 The solid histogram is for Point 5 and is the same as that shown in Figure 33 except that the binning has been changed. The hatched histogram corresponds to the point $m_0 = 90.4$ GeV, $m_{1/2} = 290$ GeV, $\tan \beta = 3.1$, $\text{sgn } \mu = -1$ and $A_0 = 66$ GeV.

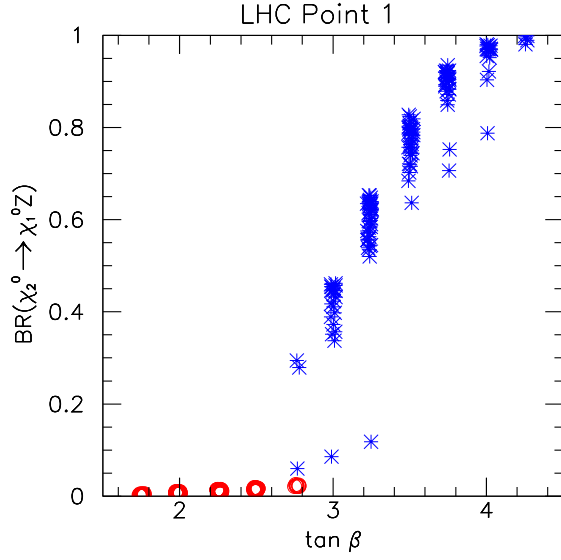


Figure 42: The branching ratio $\chi_2^0 \rightarrow \tilde{\chi}_1^0 Z$ for models with $M_h = 111.5 \pm 3$ GeV, $M_{\text{eff}} = 920 \pm 90$ GeV and both signs of $\mu = +1$ (circles) and $\mu = -1$ (crosses) as a function of $\tan \beta$.

8 Conclusions

In this paper we have outlined a strategy that can be used to systematically explore supersymmetry assuming that it is discovered at the LHC. We have given an example of a global variable (M_{eff}) that can be used to determine the mass scale of SUSY if nature has chosen the SUGRA model. Such global variables will be used to give the first indication of a signal independent of the type of SUSY model. The production of heavy mass states virtually guarantees that events with very energetic jets will exist. Other SUSY models such as those with R -parity violation [14] may have no missing E_T if the LSP decays within the detector. If the LSP decays to leptons, then all SUSY events will have leptons and they can be used in a global variable. If the LSP decays to hadrons, the jet multiplicity will rise and a variable similar to M_{eff} should be effective.

More detailed exploration will depend on the particular SUSY model. In the SUGRA models, there is a general feature, namely that the second lightest neutralino almost always decays to $h + \tilde{\chi}_1^0$ if the channel is open and to $\ell^+\ell^- + \tilde{\chi}_1^0$ with a substantial branching fraction if it is not. In the former case, this will be the dominant source of h and it will be discovered in this process via its decay to $b\bar{b}$ if it has not been seen at LEP. In the latter case the measurement of the position of the end point in the $\ell^+\ell^-$ mass distribution provides a very precise measurement of the mass difference between two of the sparticles. After first observing one of these signals, one will move up the decay chain to determine other quantities.

We have then illustrated, using specific examples, some techniques that can be used to determine masses and branching ratios of sparticles. Some of these quantities were then used to determine the fundamental parameters of the SUGRA model some of which can be determined with great precision. The ultimate goal of such studies would be to use very many measurements to make an overconstrained fit to the model, rather in the same way that current data are used to test the Standard Model [15]

The results in this paper are only an indication of the exciting physics that lies ahead for the members of the CMS and ATLAS collaborations if nature proves to be supersymmetric on the weak scale.

This work was begun during the Summer Study organized by the Division of Particles and Fields of the American Physical Society. We benefited from many discussions with attendees at that study and with colleagues on the ATLAS collaboration. In particular we would like to thank Stephan Lammel, John Bagger, Alfred Bartl, Fabiola Gianotti and Daniel Froidevaux.

The work was supported in part by the Director, Office of Energy Research, Office of High Energy Physics, Division of High Energy Physics of the U.S. Department of Energy under Contracts DE-AC03-76SF00098 and DE-AC02-76CH00016. Accordingly, the U.S. Government retains a nonexclusive, royalty-free license to publish or reproduce the published form of this contribution, or allow others to do so, for U.S. Government purposes. One of us (JS) would like to thank the Swedish National Research council for support.

References

- [1] ATLAS Collaboration, *Technical Proposal*, LHCC/P2 (1994).
- [2] CMS Collaboration, *Technical Proposal*, LHCC/P1 (1994).
- [3] H. Baer, C.-H. Chen, F. Paige, and X. Tata, Phys. Rev. **D52**, 2746 (1995); Phys. Rev. **D53**, 6241 (1996).
- [4] A. Bartl, J. Soderqvist *et al.*, to appear in *Proceedings of the 1996 DPF Summer Study* (Snowmass, CO, 1996).
- [5] D. Froidevaux and E. Richter-Was, presentation to ATLAS Collaboration Meeting (June, 1996).
- [6] H.P. Nilles, Phys. Rep. **111**, 1 (1984);
H.E. Haber and G.L. Kane, Phys. Rep. **117**, 75 (1985);
L. Alvarez-Gaume, J. Polchinski and M.B. Wise, Nucl. Phys. **B221**, 495 (1983);
L. Ibanez, Phys. Lett. **118B**, 73 (1982);
J.Ellis, D.V. Nanopolous and K. Tamvakis, Phys. Lett. **121B**, 123 (1983);
K. Inoue *et al.* Prog. Theor. Phys. **68**, 927 (1982).
- [7] F. Paige and S. Protopopescu, in *Supercollider Physics*, p. 41, ed. D. Soper (World Scientific, 1986);
H. Baer, F. Paige, S. Protopopescu and X. Tata, in *Proceedings of the Workshop on Physics at Current Accelerators and Supercolliders*, ed. J. Hewett, A. White and D. Zeppenfeld, (Argonne National Laboratory, 1993).
- [8] F. Abe, *et al.*, Phys. Rev. Lett. **75**, 11 (1995).
- [9] S. Abachi, *et al.* FERMILAB-PUB-96-177-E.
- [10] F. Abe *et al.* Phys. Rev. Lett. **73**, 2667 (1994), Phys. Rev. **D52** 2605 (1995).
- [11] S. Abachi *et al.*, Phys. Rev. Lett. **74**, 2632 (1995).
- [12] J. Ellis, *et al.*, Nucl. Phys. **B238**, 453 (1984);
A. Gabutti *et al.*, hep-ph/9602432;
H. Baer and M. Brhlik, Phys. Rev. **D53**, 597 (1996).
- [13] S. Mrenna, hep-ph/9609360.
- [14] L.J. Hall and M. Suzuki, Nucl.Phys. **B231**, 419 (1984).
- [15] See for example, D. Schaile, in *Proc. International Conference on High Energy Physics (ICHEP)*, (Glasgow, Scotland, 1994).